Aust. J. Zool., 1994, 42, 125–62

Endotherm Energetics: from a Scalable Individual-based Model to Ecological Applications

Warren P. Porter[A], *James C. Munger*[B], *Warren E. Stewart*[C], *Srinivas Budaraju*[C] *and James Jaeger*[A]

[A] Department of Zoology, University of Wisconsin, Madison, WI 53706, USA.
[B] Department of Biology, Boise State University, Boise, ID 83725, USA.
[C] Department of Chemical Engineering, University of Wisconsin, Madison, WI 53706, USA.

Abstract

We outline a computer model of heat and mass transfer through flesh, fat and porous fur for endotherms of any dimensions. We then validate it with a series of laboratory studies. Finally, we explore applications of the model to Bergmann's rule, predicting the mouse-to-elephant curve, climate–disease–toxicant interactions, animal 'design' via genetic engineering and energetic constraints on community structure.

As a first test of the model we present calculations and metabolic chamber measurements for mammals ranging in size from mice to Holstein calves. We then compare simultaneous measurements on deer mice, *Peromyscus maniculatus*, of oxygen consumption, doubly labelled water turnover and food consumption with calculations of metabolic rate using body temperature radio-telemetry as input to the endotherm model. The endotherm model derived in the Appendix requires data on allometry (body dimensions, surface area), fur properties, core temperature, air and radiant temperatures and wind speed. The model is useful for calculating energetic expenditure in different microclimates without the need for extensive physiological measurements in the laboratory. Model predictions of metabolic rate at 12°C and at 22°C were well correlated with each of the three empirical estimates. The model shows that the posture an animal assumes can influence measurements of metabolic rate. Model calculations of metabolic rate using postures ranging from a curled-up ball-like geometry to a sprawled-out, cylinder or ellipsoid geometry bracket all three sets of simultaneous empirical data taken on the same animals.

Applications of the model show that it can be applied in a wide variety of circumstances to gain insight into physiological and ecological problems.

Introduction

The evolution of endothermy and its relationship to the evolution of fur has stirred man's curiosity for a long time (Fig. 1). This early, unpublished photo of work done by Raymond Cowles was an obvious attempt to understand how fur might affect thermoregulation and body temperatures in reptiles if they had possessed fur. It was Kovarik (1964) who developed the first mathematical model that attempted to address the problems of porous fur. The development of high-speed computers and numerical methods now make it possible to solve porous media equations and to describe quantitatively how porous media function.

In biological systems mass and energy are interconnected. For example, the amount of mass consumed by an animal is related to the amount of chemical energy that can be liberated by metabolic processes in the form of heat. This connection, as well as several others, has been developed quantitatively in earlier papers as a set of coupled equations (Porter and McClure 1984; Porter 1989*a*). One important aspect of such an expression of mass and energy balances is that it illustrates how relatively few variables can govern processes at multiple levels of biological organisation.

0004-959X/94/010125$20.00

Fig. 1. Unpublished photograph of Raymond Cowles's early work on thermoregulation in reptiles as affected by fur (courtesy of Raymond Huey).

In this paper, we present models of fur and flesh heat transfer that predict metabolic heat generation of an endotherm given input of micrometeorology variables and animal characteristics, such as fur properties, body dimensions and core temperature. We then present tests of the model, followed by applications of the model to Bergmann's rule, predicting the mouse-to-elephant curve, climate–disease–toxicant interactions, animal 'design' by genetic engineering and energetics constraints on community structure.

The derivations of the main formulae are outlined in the Appendix. Details of the model derivation do not exist in the open literature. Furthermore, additions and refinements of the model after Kowalski's derivations have not been published.

The models presented here do not include solar radiation and forced convection in fur, which are substantially more complex (Stewart *et al.* 1993; Budaraju *et al.* 1994). Their implementation in the model is not yet completed. Nonetheless, the model presented here works well in metabolic chambers, at night-time or low-light conditions.

The study of endotherm energetics has a long history. Systematic research into human energetics began more than 100 years ago with the early experiments of Rubner (Rubner 1883). Shortly thereafter Lord Rayleigh (Raleigh 1892) derived important relations for various properties of structured porous media. Subsequent studies of domestic animals summarised by Brody (1945) and Kleiber (1975) contained empiricism, but also contained efforts to develop quantitative models of animal energetics. Added mathematical sophistication in the development of fur models emerged with the studies by Kovarik (1964), who used a simple scattering theory of radiation. Another approach using Ohm's law analogies of conductance and resistance was represented by the work of Scholander *et al.* (1950).

Application of engineering principles to heat and mass balance in animals has greatly aided our understanding of how environmental and animal properties interact. Biological and engineering approaches to animal energetics began to merge with the publication of

Gate's 'Energy Exchange in the Biosphere' (Gates 1962). Development of fur models accelerated with the appearance of computers that could solve the complex simultaneous equations that often required numerical solutions. Davis and Birkebak (1974) developed a model for heat transfer through fur. Their model requires a linear temperature profile in the fur, which may not always be the case (Skuldt *et al.* 1975). Their model also suffers from the assumption that heat loss through the fur layer depends only on the local temperature gradient whereas it can depend strongly on the external radiative environment (Skuldt *et al.* 1975). Cena and Monteith (1975*a*, 1975*b*, 1975*c*) also developed a fur heat transfer model. Like Davis and Birkebak, they solved the combined conduction and radiation problem and developed expressions for the effective thermal conductivity, but the resulting predictions differ from the experimental results of Skuldt *et al.* (1975). The diffusive radiation model used by Cena and Monteith (1976) is appropriate for optical thicknesses of 20 or more, but not in the range of 0–8, which is typical for fur (Davis 1972). Kowalski (1978) drew from these studies and others to develop a more general model that we use in this paper. Extensive experiments on fur-covered plates and cylinders, both indoors and outdoors (Moote 1955; Tregear 1965; Davis and Birkebak 1974), provided early tests of Kowalski's models on inanimate objects.

Development of a porous media model was important because approximations of fur as a solid medium, as done by Porter and Gates (1969), can be significantly less accurate in predicting endotherm energetics (Steudel *et al.* 1994). Fur complicates heat exchange analyses because radiation can penetrate the fur or leave it from any depth. This affects the temperature distribution within the fur. Conduction occurs along the fur fibres, but heat is also exchanged via the air spaces within the fur.

Two versions of the low-velocity fur model have been developed. One version, LOFUR, uses numerical integration within the fur to compute heat fluxes. This allows for inclusion of property variations in the fur, such as density changes with depth due to different hair lengths, curled hairs or feather structure for birds. Sensitivity analyses (McClure and Porter 1983) suggest that variation in density with depth over normal ranges is not a dominant variable affecting fur heat fluxes by conduction and radiation. A simpler model, EZFUR, used in the present paper, has an analytical solution based on a linear temperature profile with a correction factor for non-linearity (Siegel and Howell 1972). Both models include radiation–conduction processes throughout the fur and convection and radiation at the outer boundary. Free convection processes within fur and other porous media are insignificant at most wind speeds normally encountered in the field (Lapwood 1948; Rowley *et al.* 1951; Lander 1954; Wolf 1966; Tien and Cunnington 1973; Skuldt *et al.* 1975; Walsberg 1988).

The Model

The model contains coupled mechanisms of heat and mass transfer (Fig. 2). The equations shown in Fig. 2 share common terms in the heat and mass transfer equations for metabolism and evaporation (Porter 1989*a*). The equations emphasise that growth, reproduction, and fat storage depend upon (1) environmental conditions that affect heat fluxes in the diagonal heat balance equation, (2) mass ingested and absorbed which determines the amount of dry matter and water ingested and absorbed, and (3) metabolic rates and evaporative water losses that are affected by physiology (body temperature maintained) and behaviour (microclimates selected, activity levels, locomotor costs to obtain food with a distribution that changes, appetite levels).

The endotherm model is driven by a microclimate model (Porter *et al.* 1973; Mitchell *et al.* 1975). The microclimate model requires information about air temperature and wind speed at a known height, average annual temperature to specify deep soil temperature, soil properties, humidity at a known height and either measurements of solar radiation or geographic coordinates to calculate the available solar radiation for clear sky conditions (McCullough and Porter 1971; Porter 1989*b*). The microclimate model simply solves the

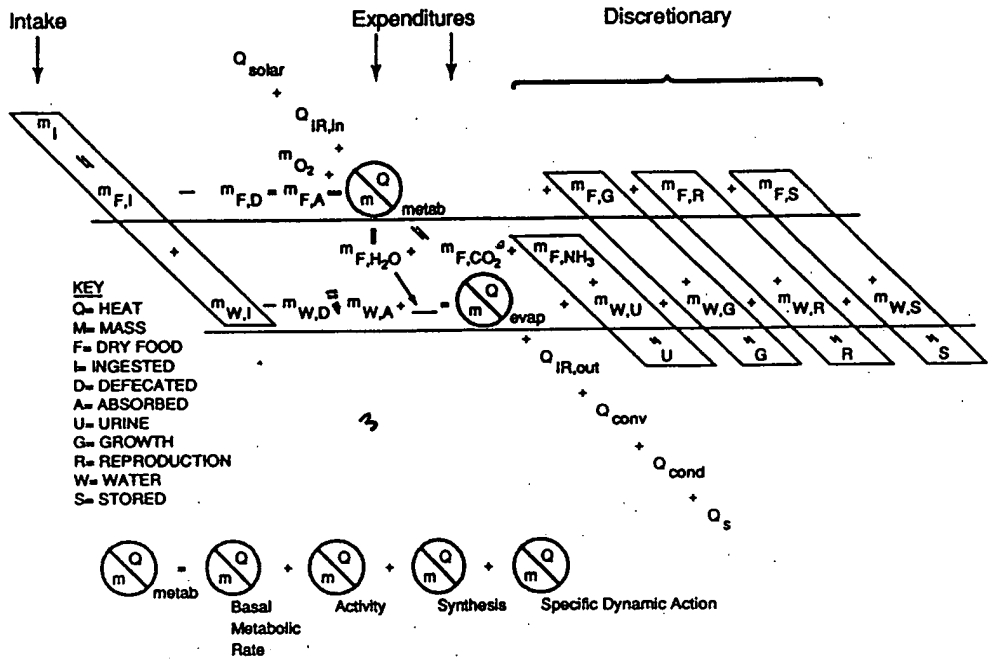

Fig. 2. Coupled heat and mass transfer equations, illustrating how the models can also be used to quantitatively evaluate energetic consequences of climate–disease–toxicant interactions, and to assess energetic constraints on community structure. Metabolic and evaporative water loss are affected by both environmental conditions through the heat balance equation on the diagonal and the horizontal dry matter and water mass balances. Discretionary mass available for growth, reproduction or fat storage is altered by changes in the environment or ingested mass and depend on the mass balance of both the dry matter and water.

energy balance at the ground surface and at user-specific depths between the ground surface and (constant = average annual temperature) deep soil temperature by means of a set of simultaneous equations that are solved numerically with an Adams Predictor-Corrector algorithm. Air temperatures and wind speeds from the ground surface upward to the 2-m reference temperature and wind speed are computed from measured or calculated profiles based on vegetation morphology (Mitchell *et al.* 1975).

The evolution of the endotherm model from the late 1960s to the present was a progression from a linear slab model to a non-linear internal heat generation model coupled to a porous fur model (Fig. 3). Below the left-most panel is a temperature profile from the centre of the animal to the edge of the solid fur. Heat in this model is presumed to be generated and released at the very centre of the animal and then conducted linearly through the animal as though it were a slab of tissue.

The next stage in evolution was the addition of non-linear heat generation for the core of the animal and accommodation of cylindrical geometries such that heat was presumed to be generated within the flesh part of the organism and conducted radially in the wedge- or cone-shaped geometry that extends from the centre of a cylindrical, spherical or ellipsoidal geometry (Bird *et al.* 1960). An assumption of non-slab geometry leads to a parabolic concave downward-temperature-profile curve from the centre of the animal to the edge of the heat-generating tissue. Heat conduction through the fat layer and the solid fur layer occurs in non-linear fashion as described by logarithmic temperature profiles (Bird *et al.* 1960). In the left and centre panels of Fig. 3 the conductivity of the fur is modelled as a solid. As such its value is constant and does not depend on any other variables.

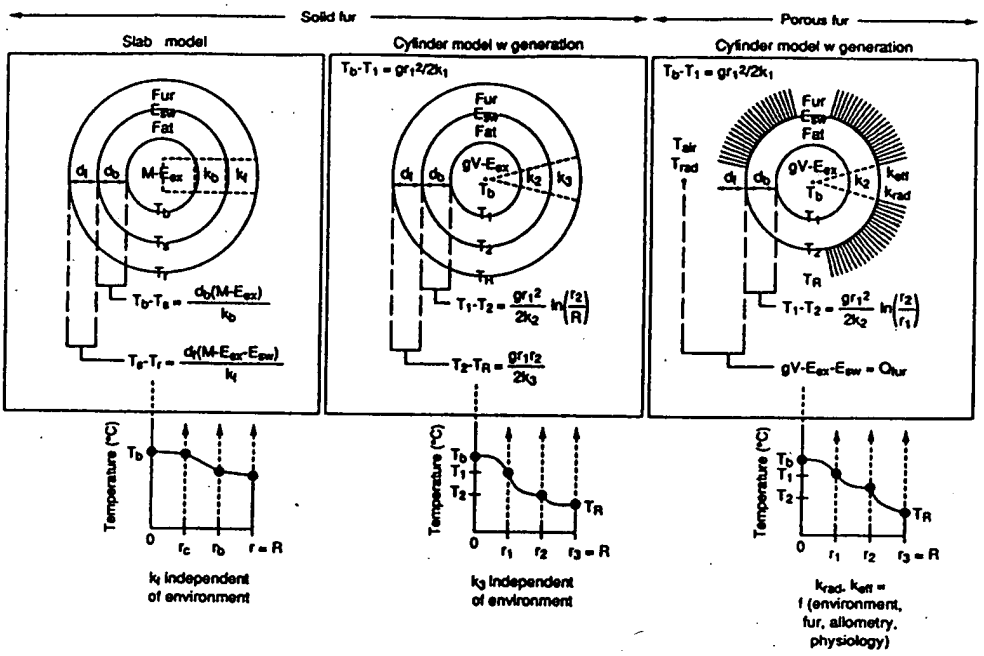

Fig. 3. Evolution of endotherm models from linear solid-fur models to non-linear porous-fur models. Different assumptions about geometry affect computed heat fluxes. 'Thermal conductivities' for radiation and conduction through fur modelled as a porous medium are not constants, but depend on many variables simultaneously. Comparisons of heat flux calculations for the same sheep show that the porous model has intermediate estimates of heat flow relative to the slab (lowest) *v.* cylinder (highest) computed flux for the same animal and environmental parameters. The left-most panel is from Porter and Gates (1969).

The current version of the fur model illustrated in the right panel of Fig. 3 incorporates the porous nature of fur, where there is heat transfer by conduction along hair fibres and through the air columns between the fibres, as well as by infrared radiation diffusely emitted, absorbed and re-emitted between the hair fibres in the fur in the outgoing and incoming directions. A model for absorption of the solar radiation by diffuse reflection and transmission within the fur has also been developed (Kowalski 1978). The effective conductivities for conduction processes and radiation processes, k_{eff} and k_{rad} depend upon many variables simultaneously (bottom right of Fig. 3). That is, environmental conditions, animal body size, fur properties such as hair length, diameter, density and pelt depth all simultaneously affect heat loss through fur and therefore the metabolic heat (and food) needed to maintain that heat loss. Temperature profiles affect heat transfer rates and so the geometry assumed and the associated equations are important in estimating computed heat fluxes for known physical properties. A comparison of these three models for a sheep shows that the porous fur model is intermediate in its estimate of heat fluxes, with the linear model underestimating and the solid cylindrical model overestimating heat loss (Steudel *et al.* 1994).

Recent work by Stewart *et al.* (1993) and Budaraju *et al.* (1994) has produced a model for fur that calculates wind flow and convective processes of heat and mass transfer through porous media. Velocity profiles calculated through two different types of fur are shown in Figs 4 and 5. These calculations show that the movement of air through fur at high external wind speeds is confined to the front half of the animal that is facing the wind.

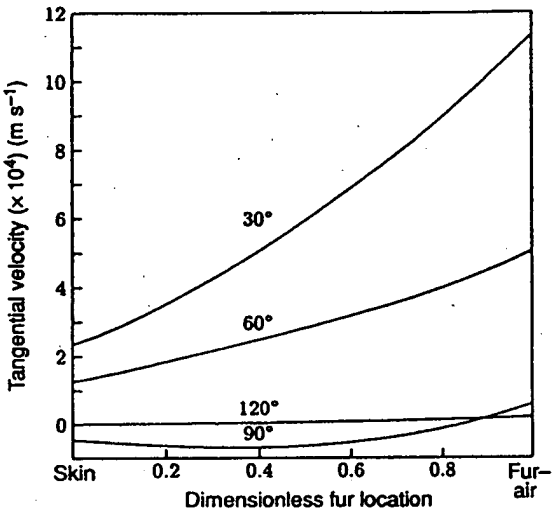

Fig. 4. Computed velocity profiles through the dense fur of the eastern gray squirrel, *Sciurus carolinensis*, at free stream wind of 2 m s^{-1}, using the first principles forced convection model of Budaraju *et al.* (1994).

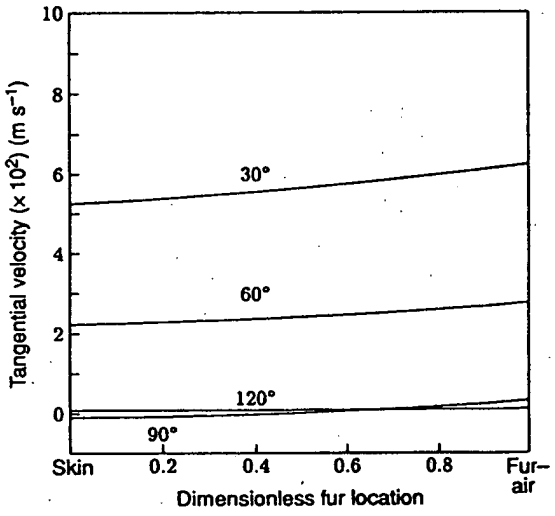

Fig. 5. Computed velocity profiles through the more sparse fur of the European red deer, *Cervus elaphus*, at free stream wind of 2 m s^{-1}, using the forced convection model of Budaraju *et al.* (1994).

The downstream half of the animal has air movement in the fur that is so low as to be essentially still air. Thus, the back half of the animal relative to wind direction can be treated as a conduction–radiation problem, whereas the front half of the animal should be treated as a conduction–convection–radiation problem, if there is sufficient wind speed to induce flow through the fur. Whether flow occurs depends upon the animal's size, external wind speed, and fur properties. This is automatically determined by the model.

How the computer program determines metabolic rate of an endotherm is illustrated in Fig. 6. Given a core temperature to be maintained, the radial dimension of the animal from the centre of the animal to the edge of the generating tissue (assumed for simplicity in this case to be the skin of the animal), the fur properties, and the environmental conditions of solar and infrared radiation, air temperature, wind speed and humidity, there is one and only one metabolic heat production rate that will satisfy those conditions. The infrared radiation from the ground is determined by the ground surface temperature. That temper-

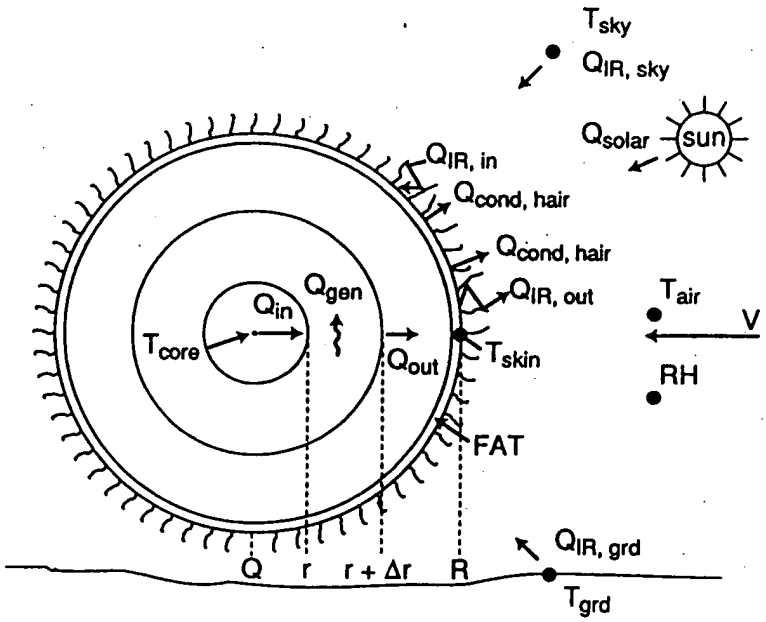

Fig. 6. System diagram used to illustrate the variables that affect required heat generation to maintain a defined core temperature. The amount of heat that must be generated depends on the radial dimensions of the animal, surface area and volume, fur properties and environmental conditions.

ature is obtained from microclimate simulations solved prior to the animal heat balance problem. The wind speed incident on the animal is determined by the microclimate calculations done at all heights up to the reference height, 2 m. So, no matter where the animal goes above the surface or below the surface, environmental conditions can be estimated.

The computer program, EZFUR, consists of three models: one for heat transfer in heat-generating tissue, one for any insulating tissue and one for heat transfer through porous fur (Porter *et al.* 1986). They are solved simultaneously by computer iteration to determine the heat generation (i.e. metabolic rate) needed to maintain a specified (regulated) core temperature. The parameters and variables needed for the solution in an environment without significant sunlight, such as a metabolic chamber, night or shade conditions are a specified core temperature, body radius, surface area, four fur properties (hair density, length, diameter and pelt depth), and environmental conditions of air and radiant temperatures and wind speed (Porter 1989*a*). If water loss by respiration or by other means is a significant variable and part of the endotherm model, humidity must also be known.

The basic structure of EZFUR used in this paper is shown in Fig. 7. MAIN is primarily involved in input/output (Table 1) and control of subroutines. ALLOM performs calculations of animal dimensions, area and volume from input data and regressions based on weight. FURPRO supplies the fur properties of the animal being modelled. REGFAL is a *regula falsa* guessing routine (Press *et al.* 1987) that repeatedly calls function FUN in the process of guessing a parameter value (heat generation per unit volume in this case) until the heat balance equation (Equation 53 in Appendix) balances. FUN is a function that contains the temperature-dependent energy balance equation described in the Appendix. FUN calls E4, which computes exponential integrals (Abramowitz and Stegun 1968) needed for calculating the simultaneous inward and outward radiation fluxes in the fur. It also calls

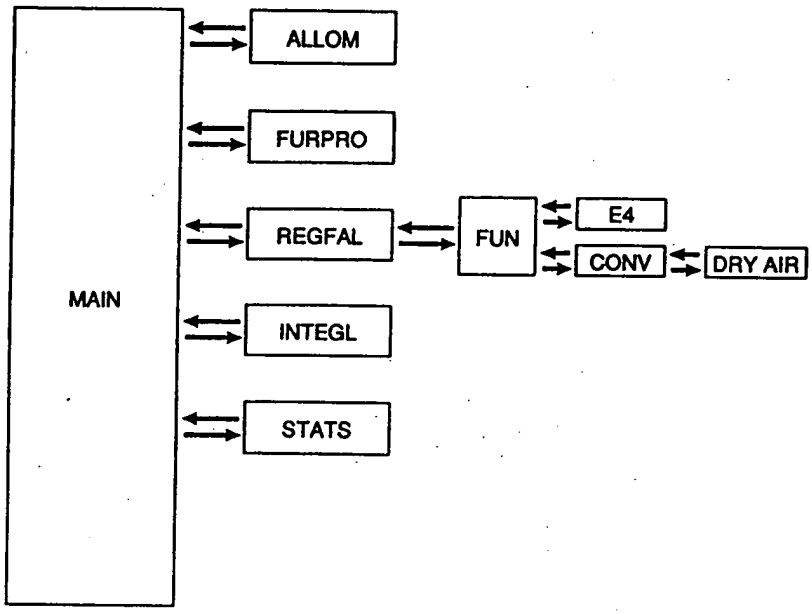

Fig. 7. Flow chart of the computer program EZFUR. Subroutine ALLOM calculates surface area and body radius from weight using species specific regressions or geometric approximations. FURPRO sets species specific dorsal and ventral fur properties. REGFAL is a Regula Falsa guessing routine that guesses a heat generation by the body that satisfies the time-dependent core temperature obtained by telemetry, body dimension and skin surface area, fur properties and environmental conditions by balancing the energy balance equation in FUN. E4 contains exponential integrals for solving the diffuse radiation transfers in and out of the fur. CONV calculates convective heat transfer at the fur–air interface as a function of wind speed, air and fur tip temperature and total body diameter including fur. INTEGL integrates metabolic rate over time and STATS computes test statistics.

Table 1. Sample variables for the endotherm model

Animal variable	Sample high value	Sample low value
Hair diameter (m)	$1{\cdot}16\times10^{-5}$	$1{\cdot}04\times10^{-5}$
Hair length (m)	$6{\cdot}40\times10^{-3}$	$3{\cdot}84\times10^{-3}$
Hair density (hairs m^{-2})	$1{\cdot}19\times10^{8}$	$7{\cdot}12\times10^{7}$
Pelt depth (m)	$4{\cdot}86\times10^{-3}$	$4{\cdot}23\times10^{-3}$
Environmental variable	**Sample value**	
Air temperature (°C)	22	12
Radiant (wall) temperature	22	12
Relative humidity (%)	90	10
Wind speed ($m\ s^{-1}$)	10·0	0·1
Altitude (m)	0	0

CONV, a general convection-heat-transfer subroutine for various geometries. CONV calculates convective heat loss at the fur–air interface. CONV calls DRYAIR, which contains the physical properties of dry air as a function of air temperature (Tracy *et al.* 1980). The

user may alternatively elect to provide a convection subroutine based on experimental wind tunnel data for a particular animal, so ANCORR may optionally be called from CONV to substitute the Nusselt-Reynolds correlations for standard geometries (flat plate, cylinder, sphere, ellipsoid) (McAdams 1954) for a specific animal shape. When the user is uncertain as to which shape to use, a sphere is a good approximation. Mitchell (1976) showed that spherical approximations have good agreement over a broad range of animal sizes, if the characteristic dimension used is the cube root of the volume.

Derivation of the function that connects microclimate variables and skin temperature, T_{sk}, is given in the Appendix. Core-skin temperature gradients generated from heat released as a result of metabolic processes are non-linear. Linear relationships between core and skin temperature, such as used in Porter and Gates (1969) are more convenient mathematically, but may be inappropriate, especially for larger body diameters, where the temperature gradient may be substantial. Skin temperature is related to core temperature, T_c, by the non-linear equation

$$T_c - T_{sk} = \frac{gR^2}{nk} \quad (1)$$

where n is an integer of value 2, 4 or 6, depending on whether the geometry is a flat plate, cylinder or sphere (Bird *et al.* 1960; Kreith and Black 1980). An ellipsoid has n equal to 2 and all three semi-axes are a part of the solution and appear raised to the second power (Appendix). R is the dimension from the centre to the outer edge of the heat-generating tissue. Flesh thermal conductivity, k, and heat generation per unit volume, g, constitute the other relevant variables.

At the end of the calculations for each hour, MAIN calls INTEGL, a trapezoidal integration routine that computes total hourly metabolism. At the end of a day, MAIN calls STATS to compute daily means and standard errors.

Materials and Methods

To test the validity of predictions made from the model, we performed laboratory experiments in which we simultaneously (i) measured those parameters necessary for EZFUR to calculate metabolic rate (body temperature, T_b; air temperature, T_{air}; and radiant temperature, T_{rad}), and (ii) used three independent methods to estimate metabolic rate. Eight deer mice, *Peromyscus maniculatus bairdii*, were subjected to two measurement periods, one at an air and wall temperature of 12°C and one at 22°C. During each measurement period, metabolic rate was estimated by gas respirometry, doubly labelled water and mass balance.

Mice were housed individually in air-tight stainless-steel chambers with glass lids (23 × 12 × 13·5 cm). Fluorescent light enters the cage via its glass lid. A small enclosed nest box (8 × 8 × 8 cm), filled to a depth of 2 cm with wood shavings, was attached to the inside of each chamber. The remainder of the cage floor was a stainless-steel 6·5-mm mesh screen floor. Urine and faeces fell through the screen floor and collected under a layer of mineral oil. Purina mouse chow and water were provided *ad libitum*. The cages were housed in an environmental chamber (Environtrol Model E28XL; Puffer-Hubbard, Grand Haven, MI), allowing control of temperature and photoperiod.

Air, preconditioned to a dew point of 0°C, entered each cage through three holes spaced 13 cm from each other in the glass lid. Air was drawn out through a 0·5-cm inside-diameter hole connected to stainless-steel tubing in each of three sides. The holes in the sides were 6 cm from the bottom and flush with the wire mesh screen supporting the mice. This configuration was used to obtain good mixing of the air in the chamber as judged by smoke injection. A switching manifold caused the air from each

chamber to be exhausted through a ventilation pump for 24 of every 30 min. For the remaining 6 min, air from a chamber was drawn through a series of sensors.

First, dew point was measured with a Model 911 digital humidity analyser (EG&G, Waltham, MA), then mass flow with a Linde model FM-4550 mass flow meter (Union Carbide Corp., Somerset, NJ). Following desiccation by drierite, the air was analysed for oxygen content using a 2-channel model S-3A oxygen analyser (Applied Electrochemistry Inc., Sunnyvale, CA) and for CO_2 content using a Model 864 infrared analyser (Beckman Instruments Inc., Fullerton, CA). Air and surface temperatures were measured using thermistors (Yellow Springs Instruments, Yellow Springs, OH).

Analog output from all sensing devices was converted, using previously derived calibration relationships, to true values of dew point, mass flow, oxygen content, and CO_2 content, which were then stored by an Apple IIe computer. Atmospheric pressure was measured with a mercury barometer. Washout time from the switching manifold through the sensors is approximately 45 s. Values from the first 2 min of each 6-min sampling period were discarded to prevent carry-over from one chamber to the next. Body temperature was recorded more or less continuously, using temperature-sensitive AM transmitters (Model XM-FH, Mini-Mitter, Sunriver, OR) implanted intraperitoneally.

We performed experiments with two sets of 4 mice (8 total) each weighing approximately 20 g at each of two temperatures. Each set of mice was subjected to the following experimental protocol. Body temperature transmitters were surgically implanted, and the mice were allowed to recover for a minimum of 3 days. Mice were acclimated to the metabolic chambers held at 22°C for at least 4 days. Each mouse was then injected with 0·1 mL 95% $H_2^{18}O$ containing 40 μCi of ^3H_2O. After 1 h (sufficient for equilibration of the isotopes with body fluids; Degen *et al.* 1986), a 180-μL blood sample was drawn from the suborbital sinus. The mouse was then placed in its metabolic chamber. At 24 and 72 h after the initial blood sampling, blood samples were taken as above.

Food consumption was measured by weighing food available before and after an experimental run. The mice were subjected to an ambient temperature of 12°C and, after a 4-day interval, the above procedures of injection of isotopes and blood sampling were repeated.

Calculation of Observed Metabolic Expenditure

Each of 8 mice was subjected to two experimental runs, one at 22°C and one at 12°C, as described above. During each run we (i) measured food consumption and body mass to allow calculation of metabolic rate via mass balance, (ii) collected blood samples for isotopic measurement to allow calculation of metabolic rate via the doubly labelled water method, (iii) measured oxygen consumption and carbon dioxide production to allow for calculation of metabolic rate via respirometry, and (iv) measured body temperature by radio-telemetry and ambient temperature by thermistors to allow prediction of metabolic rate using the endotherm model.

To make measures from these methods comparable, all measures were converted to the mean metabolic rate between the initial and final blood samples, measured in mL CO_2 g^{-1} h^{-1}, where g is grams of body mass.

Food Consumption

In animals that are neither gaining or losing mass, respiratory expenditure must equal assimilated intake. Thus, with a knowledge of rate (or total amount) of food intake, energy content of food, and assimilation (digestive) efficiency, a rough measure of metabolic expenditure can be calculated. Total food intake during the sampling period was measured gravimetrically. Energy content of the food was assumed to be 17·8 kJ g^{-1} (4·25 kCal g^{-1}), based on Purina publications. The composition of Purina certified rodent chow is (as stated by the manufacturer) 59·7:12·22:19·44:8·68 carbohydrate:fat:protein:fibre and ash (by mass). Using tables in Nagy (1983) we calculate that an animal on this diet should produce 22·2 J per mL CO_2.

Assimilation efficiency (here measured as apparent dry-matter digestibility) was measured in a separate experiment in which 10 mice were housed individually over wire screen for a 5-day period. During this time, food consumption and faecal production were measured. Apparent dry matter digestibility (which is virtually synonymous with energy digestibility for rodents eating laboratory rations; Robbins 1983) was calculated to be

$$\frac{M_{FO} - M_{FE}}{M_{FO}}$$

where M_{FO} and M_{FE} correspond to the dry mass of food and faeces, respectively. A value of 81% was thereby obtained for assimilation efficiency. Thus, a mouse should produce 649·5 mL CO_2 per g of food consumed.

Respirometry

Hourly average rates of CO_2 production were used to calculate mean rate of CO_2 production during the interval between initial and final blood sampling.

Doubly Labelled Water

Initial and 72-h blood samples were microdistilled as described by Wood *et al.* (1975). ^3H_2O concentration was determined by liquid scintillation. ^{18}O concentration was determined as follows. First, a measured amount of distilled water from the sample was placed into a glass tube containing 7–10 μmoles of CO_2. The glass tube was flame sealed. After equilibration for 48 h at a standard temperature, the ^{18}O concentration of the CO_2 reflected that in the distilled sample. Then, in a vacuum distillation apparatus, the CO_2 was collected in the absence of water. A Finnegan model Delta E mass spectrometer was used to measure the relative molarity of ^{16}O and ^{18}O. Total metabolic expenditure between initial and final blood samples was calculated using the formulas of Nagy (1983). These calculations require knowledge of the total body water for each mouse, which was calculated using isotopic dilution (Nagy 1983). In two cases in which an abnormally low percentage body water resulted (more than 2 standard deviations below the mean), we calculated total body water using the value of mean percentage body water of the remaining mice.

Calculation of Metabolic Rates from EZFUR

Hourly values of body temperature, T_b, and air temperature, T_{air}, were the primary input into the EZFUR program. The effective radiant temperature (T_{sky}, T_{grd}) was the temperature of the walls of the respirometer chambers, and was equal to air temperature. Fur characteristics were assumed to be equivalent to those given in Conley and Porter (1986).

Three different body configurations were run using EZFUR: (i) spherical, appropriate to a mouse that has curled up, (ii) cylindrical, appropriate to a mouse sitting or lying with legs pressed to the body, and (iii) cylindrical with appendages, appropriate to an alert mouse with its appendages extended. EZFUR calculated hourly values of metabolic rate in watts. These values were integrated and converted to mL CO_2 g^{-1} h^{-1}, using 22·2 J per mL CO_2 to yield a predicted average metabolic expenditure during an experimental run.

Results

Measured respiration based on doubly labelled water turnover was very similar to respirometry values. Measurements of total respiration from each of the 16 experiments derived from doubly labelled water *v.* measurements from respirometry are compared in Fig. 8. Each of the data points are the average of all measures for an individual mouse over 72 h. The lower eight data points are for mice at 22°C and the upper eight data points are averages of all measures from eight individual mice at 12°C.

Measured respiration based on food consumption was very similar to respirometry values. In Fig. 9, measurements of total respiration from each of the same 16 experiments as those shown in Fig. 8 are compared, but derived from estimates of metabolic rate from food consumption mass balance *v.* measurements from respirometry. The left-most eight data points are averages of all measures for individual mice at 22°C. The right-most eight data points are averages for individual mice at 12°C. A line of equivalence whose slope is one is included as a frame of reference.

To calculate respiration we used hourly averages of telemetered body temperatures as input to the model EZFUR. The calculated values bounded respirometry values and suggest posture changes at different temperatures. Calculations of heat production from EZFUR, assuming three different geometries with the same total body mass (a cylinder and appendages, a cylinder approximation and a sphere approximation for each individual),

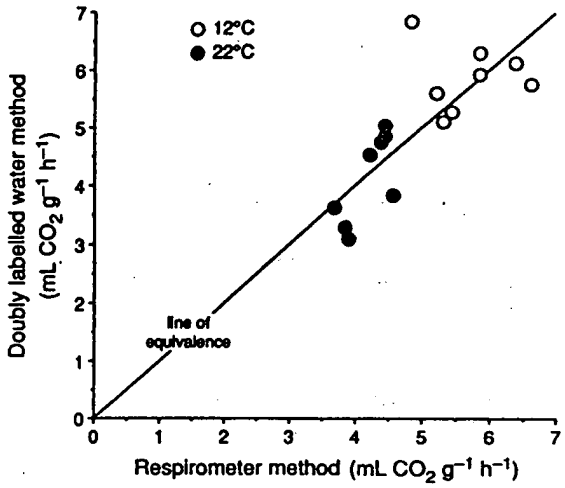

Fig. 8. Comparison of simultaneous measurements of the metabolic rate of the deer mouse by the doubly labelled water method *v.* the respirometry method at uniform air and wall temperatures of 12 and 22°C.

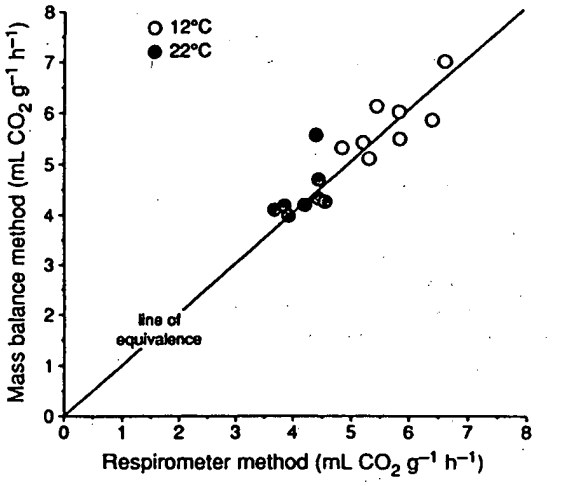

Fig. 9. Comparison of simultaneous measurements of the metabolic rate of the deer mouse by food consumption mass balance *v.* respirometry at uniform air and wall temperature of 12 and 22°C.

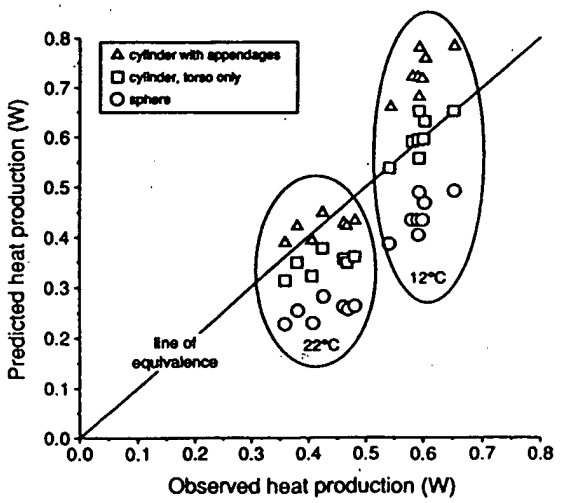

Fig. 10. Comparison of calculated heat production (22·2 J mL CO_2) using different geometries ('postures') in EZFUR *v.* observed CO_2 production (converted to J s^{-1}) in deer mice. Calculations at 22°C agree best with an assumed-cylinder-with-appendages approximation, whereas the calculations at 12°C agree best with an assumed-cylinder approximation, implying a more curled-up posture at lower temperatures.

are presented in Fig. 10. The left ellipse encloses mice held at 22°C. The right ellipse encloses mice held at 12°C. Calculations were done for only 7 of the 8 mice at 22°C because of technical difficulties with one of the temperature-sensitive transmitters. Each empirical observation on the abscissa has three predicted metabolic rates for that animal, based on the range of feasible postures. At 22°C the line of equivalence passes through the computations for a cylinder with appendages. At 12°C the line of equivalence passes through calculations assuming a cylinder without appendages. Respirometry values were converted to equivalent heat production, assuming 22·2 J per mL CO_2 produced.

Calculations of heat production by EZFUR based on hourly averages of body temperature telemetry bounded respirometry values averaged over each hour. Several examples of observed hourly respirometry data throughout a 72-h experiment (solid dots) with the hourly predicted metabolic rates from EZFUR for the three different geometries (solid and dashed lines) for air temperatures of 12°C are presented in Fig. 11. The calculated metabolic rates for each hour vary because body temperature varied accordingly. The respirometry data show variation that exists within and among individuals in level of activity over time. At 12°C, the metabolic rate data of Mouse 2 falls between the sphere and the cylinder approximation. Mouse 3 data show little variation and are close to the cylinder approximation. Mouse 4 data are also centred on the cylinder approximation by EZFUR, but the variance of the data is higher.

Analogous respirometry data and calculations by EZFUR at an air temperature of 22°C indicate a different behaviour and posture (Fig. 12). Mouse 1, 2 and 4 data fall between the cylinder with appendages and the cylinder approximation for the first half of the experiment and then the data are centred on the cylinder approximation.

Model Tests

Sensitivity analyses using this model (McClure and Porter 1983) indicated that core or skin temperature were among the most sensitive variables affecting heat loss from an endotherm. That is, a lower skin or core temperature should allow an animal to save considerable amounts of heat. Accordingly, we undertook field experiments with prairie dogs (Bakko *et al.* 1988) that showed (Fig. 13) that body temperatures on both a daily and seasonal basis changed. Calculations showed that these body temperature changes allowed for at least a 10% savings in energy as opposed to maintaining a constant core temperature. Additional data not shown here revealed that as the months got colder, body temperatures declined even further. Moreover, activity patterns also shifted seasonally to take advantage of appropriate thermal habitats above and below ground. At warmer summer temperatures activity was greatest in the cooler hours of daylight. In cooler months, most activity shifted to the middle of the day.

A variety of experimental tests in the laboratory and in the field have been done to evaluate how well the endotherm model estimates metabolic expenditures. The first of these tests was done by Gebremedhin *et al.* (1981). Calculations *v.* measurements done on one-week-old and eight-week-old Holstein calves under controlled environmental conditions are illustrated in Fig. 14. These calculations can be used to estimate growth or reproduction potential given any known amount of food or energy ration (Fig. 15). The difference between available food and energy *v.* the energy that must be expended for thermoregulation and/or activity is what is available for growth or reproduction. It is the potential for growth and reproduction that is an important part of the much broader problems of population dynamics and community structure (Adolph and Porter 1993).

The performance of the model for cotton rats in comparison with empirical data from work by Scheck (1982) is shown in Fig. 16. The calculations for two postural extremes of extended *v.* curled up (cylinder *v.* sphere approximations) suggest that at lower temperatures the animals may have been more curled up and as temperatures rose postures may have shifted more to extended configurations.

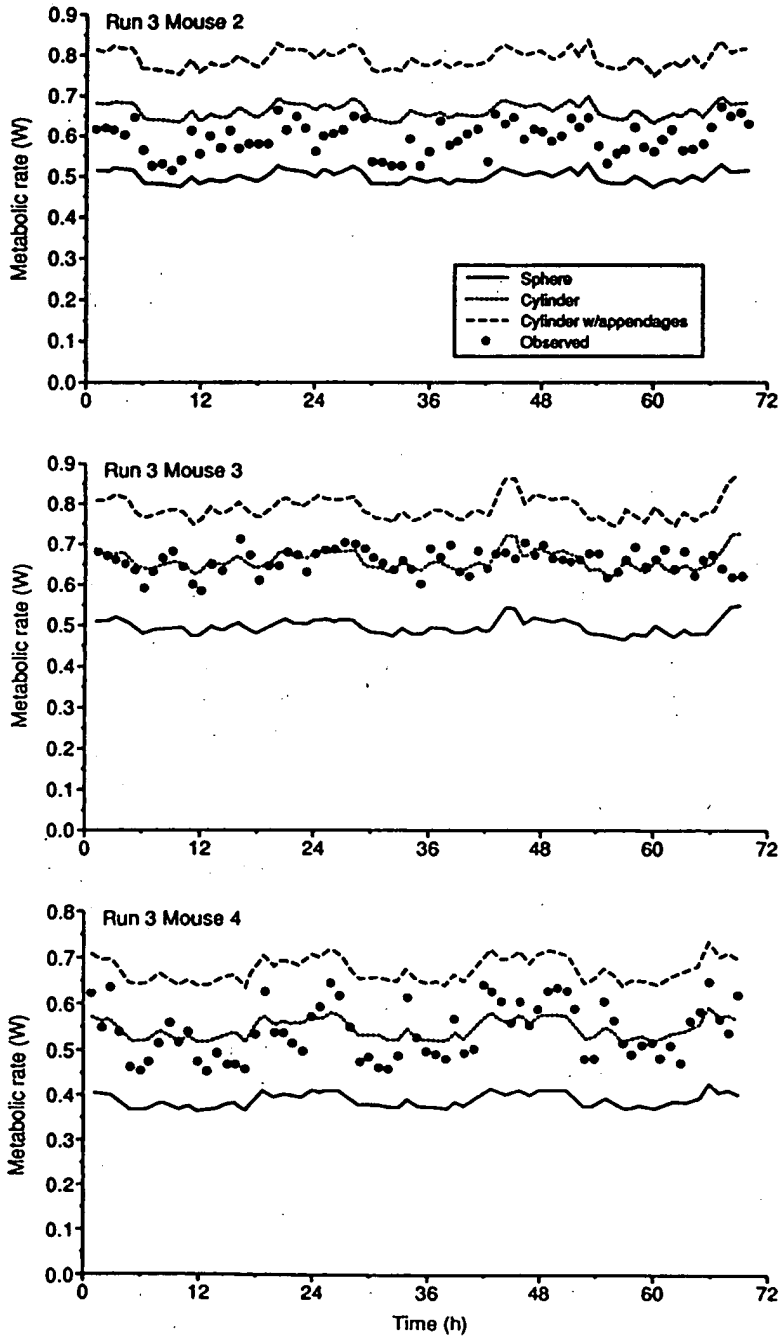

Fig. 11. Comparison of continuous measurements of the metabolic rate of the deer mouse at an air temperature of 12°C *v.* calculations based on core-temperature telemetry with program EZFUR, using three different 'postures'. Individual variation between mice show different variances in the data, but all three animals' measurements fall closest to the cylinder approximation or between the cylinder and sphere approximations of EZFUR.

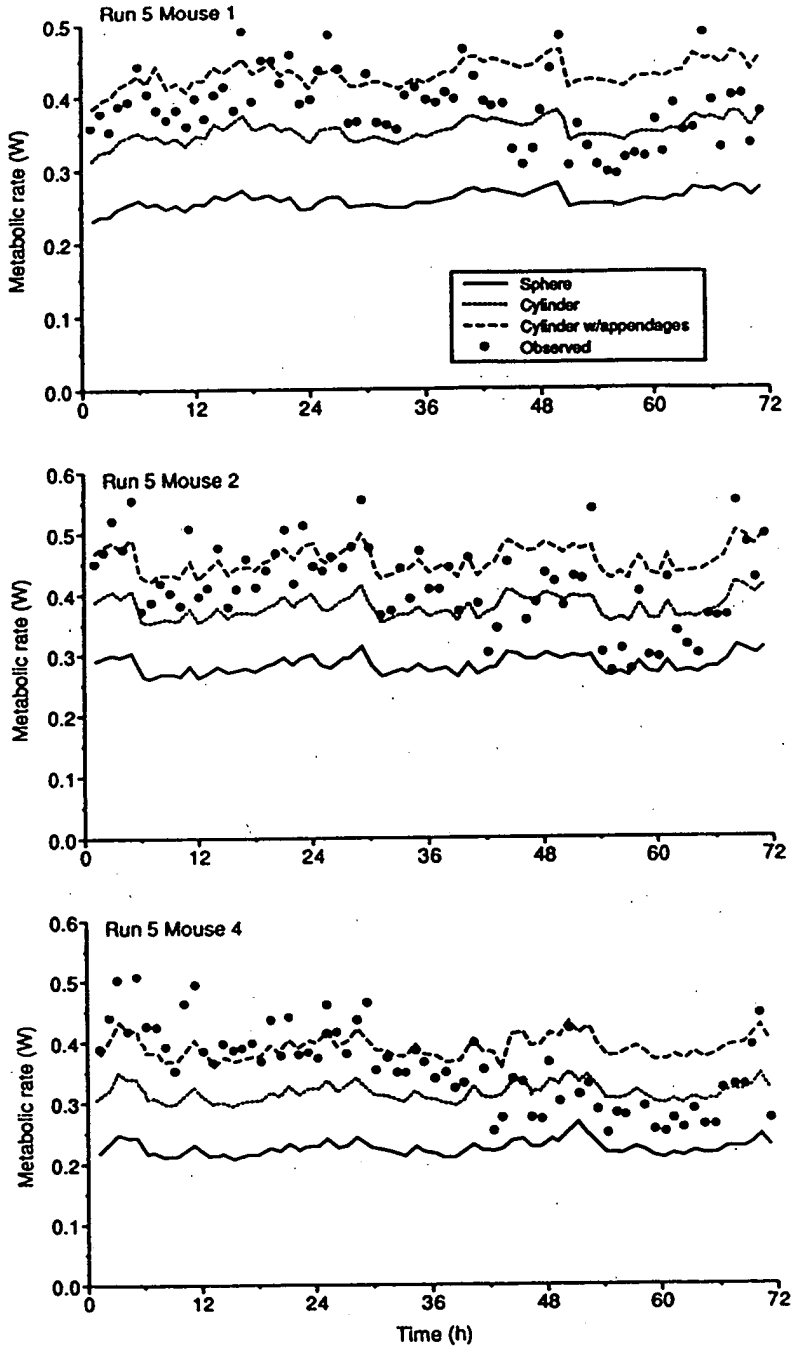

Fig. 12. Comparison of continuous measurements of the metabolic rate of the deer mouse at an air temperature of 22°C *v.* calculations based on core-temperature telemetry with program EZFUR, using three different 'postures'. Experimental data fall closer to the cylinder-with-appendages approximation, but variation of posture with time is suggested by the data.

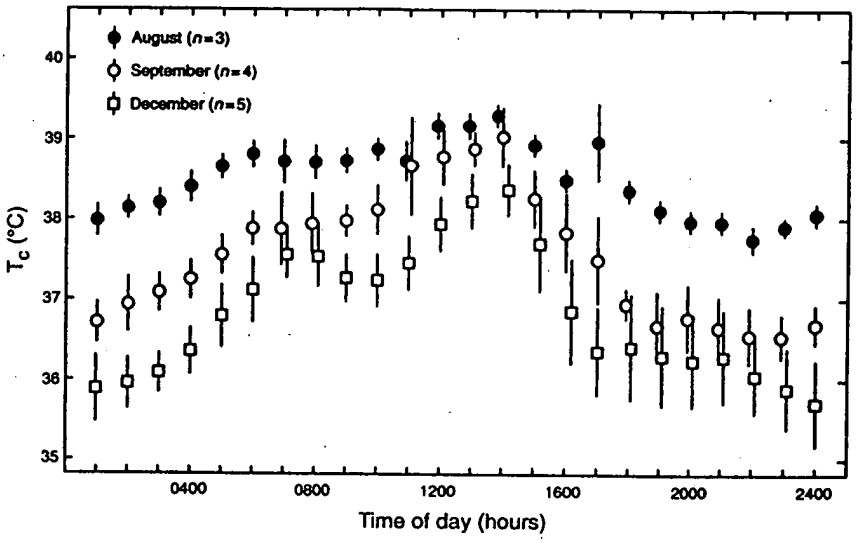

Fig. 13. Changes in regulated core temperature by day and season in the black tailed prairie dog, *Cynomys ludovicianus*, at Fort Collins, Colorado.

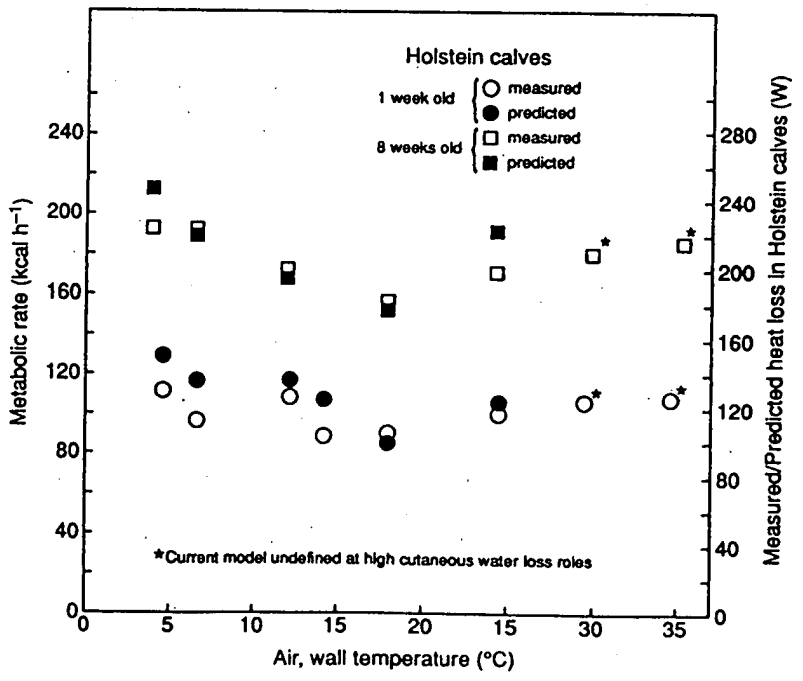

Fig. 14. Calculated *v.* measured metabolic rates in Holstein calves in the Biotron, a controlled environment facility.

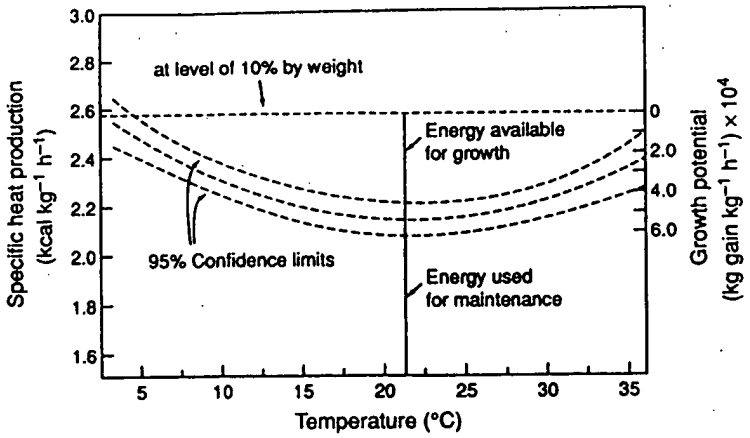

Fig. 15. Discretionary mass available for growth at any temperature due to energy absorbed *v.* energy expended by a Holstein calf.

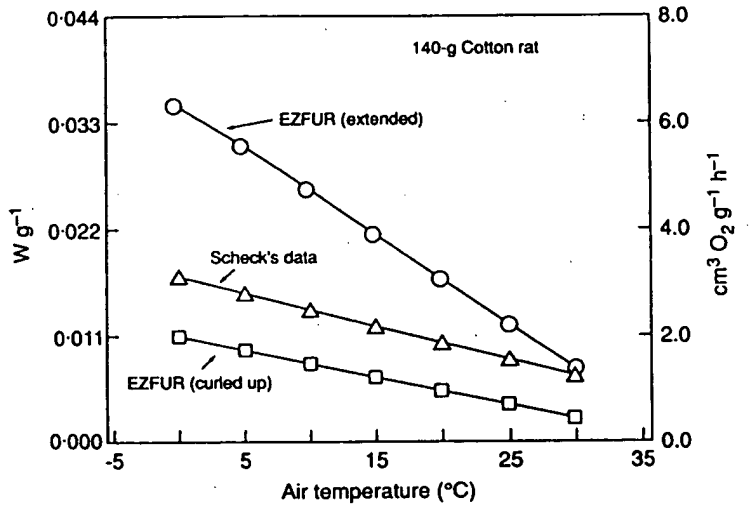

Fig. 16. Calculated resting metabolic rates for adult cotton rats, *Sigmodon hispidus*, for bounding postures of curled-up *v.* extended *v.* measured values.

Analogous calculations done with yellow bellied marmots (Fig. 17). Calculations done in collaboration with Dr Jaye Melcher are compared against empirical data by (Armitage *et al.* 1990).

Measurements and calculations done for field active singing voles at Toolik Lake on the North Slope of Alaska (Fig. 18) are from unpublished work with Dr Steve Beaupre. Calculations for the animal assume it was inactive with extended or curled-up postures. The calculated metabolic rates lie below the metabolic rates determined by field measurements using doubly labelled water assayed in our laboratory. As might be expected from the work of Degen *et al.* (1986) and others, the field active voles had higher metabolic expenditures than estimates for an animal resting in a laboratory setting.

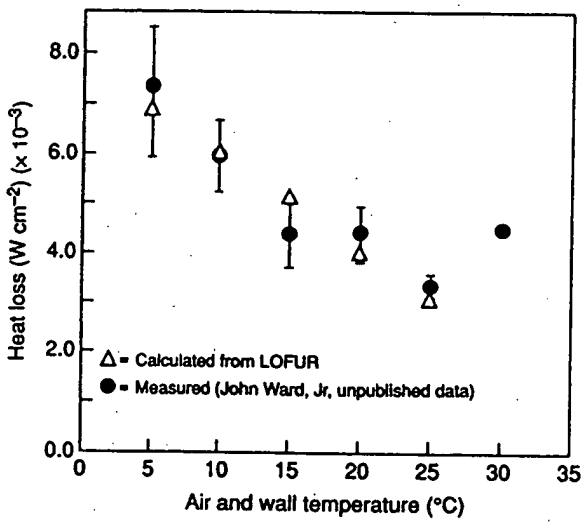

Fig. 17. Calculated *v.* measured metabolic rates for adult yellow bellied marmots, *Marmota flaviventris*, for resting conditions.

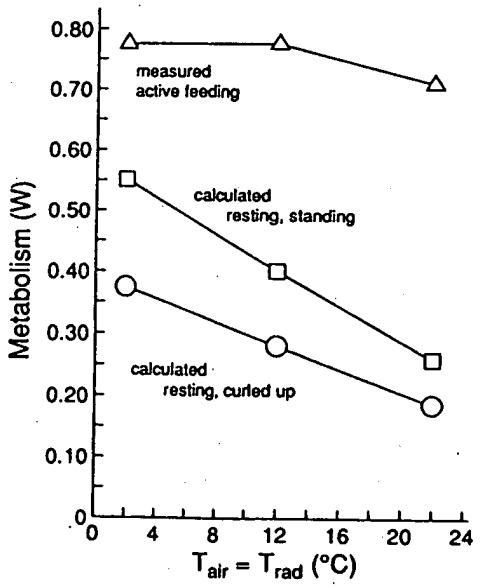

Fig. 18. Calculated resting metabolism for curled-up and extended postures *v.* field-measured metabolic rates of 28-g active adult singing voles, *Microtus miurus*, using the doubly labelled water method. T_{core} = 38°C, $v = 0{\cdot}1$ m s^{-1}.

Conley and Porter (1986; fig. 1) illustrate much more substantial tests of the model under carefully controlled conditions where evaporative water loss was partitioned between respiration and cutaneous losses and oxygen consumption and CO_2 production were measured continuously. Data obtained from this apparatus were used to compare against calculations shown in Fig. 19. The error bounds (Fig. 19) are those expected on the basis of errors in experimental measurement as a result of variation in instrumentation readings.

Subsequent to these experiments even more tests described above were done using simultaneous, independent estimates of metabolism in deer mice. These included simultaneous doubly labelled water, food consumption and gas respirometry measurements of the same individuals. In addition, simultaneous radio-telemetry of core temperature of the same individuals was done on a continuous basis to provide the data needed for computer simulations of metabolic rate.

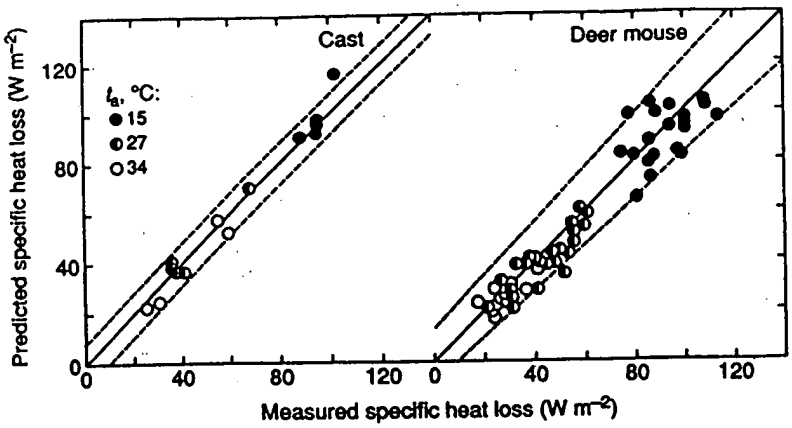

Fig. 19. Calculated *v.* measured heat loss for a fur-covered casting of a deer mouse and for live deer mice (Conley and Porter 1986), under different environmental conditions.

In summary, the endotherm model metabolism calculations bound observed metabolic data when tested on animals ranging in size from deer mice to Holstein calves and when tested on fur ranging from the the relatively sparse fur of cotton rats to dense furs of marmots and tundra voles. The model suggests that posture is an important variable in controlling heat loss. It predicts substantial energy saving for relatively modest care and skin temperature reductions. It also suggests changes in activity patterns with seasons to minimise mass and energy losses. When combined with known intake rates of gut-processing models, it can be applied to predict growth and reproductive potential in outdoor environments.

Model Applications

Bergmann's rule

The development of the endotherm model and laboratory and field tests of the model suggest that a good allometric approximation for bounding estimates of metabolic rate is a cylindrical approximation. Bergmann's rule suggests that at higher latitudes, body size increases to reduce the weight-specific metabolism. The fur model can now allow us to assess whether body-size changes or fur-property changes might be more important and under what circumstances they might be important. Fur properties from deer mice, lemmings and red deer for summer and winter pelages (Steudel *et al.* 1994) are presented in Table 2. There are very few data in the literature that describe all four fur properties needed as inputs to the endotherm model. Our laboratory has measured fur properties of deer mice for summer and winter. Dr Penny Reynolds, while in our laboratory, determined fur properties of

Table 2. Seasonal changes in fur properties of three mammals

Hair, fur	Deer mouse		Lemming		Red deer	
	Summer	Winter	Summer	Winter	Summer	Winter
Diameter (μm)	30	30	37·5	42·5	146	15
Length (mm)	9·02	8·94	12·7	19·35	22	53
Depth (mm)	6·62	6·57	6·4	11·5	4·5	29
Density (No. cm^{-2})	11820	12120	12803	25800	833	4742

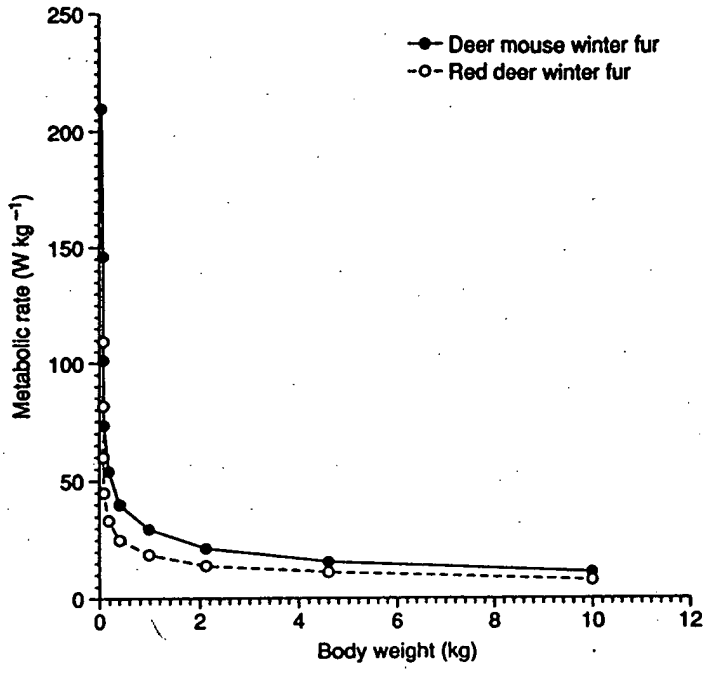

Fig. 20. Bergmann's rule calculations of weight-specific metabolic-rate changes due to body size or fur-property changes.

lemmings and was kind enough to share them with us. The data from red deer were derived from Sokolov (1982). These data suggest that there are two major differences between the fur of small and large animals.

Fur diameter in small mammals tends to change very little with season, but for a large animal like the red deer, summer hairs are thick but winter hairs are very thin. Major differences also occurred in the fur densities of small and large animals with season. Densities are extremely high for deer mice and lemmings, but the deer mouse does not change fur density greatly with the season. On the other hand, fur density of red deer changes substantially with the season. Its density changes from very sparse fur in the summer to much denser fur for the winter. Now we can ask, 'How much do body size increases *v.* fur changes affect heat loss?'.

Calculations shown in Fig. 20 were done using Meeh's equation for surface area as a function of body weight (Calder 1984). We assumed a cylindrical geometry and assumed that the length of the animal is twice the diameter. We assumed that the core temperature of the animal remained at 39°C. As Equation 1 shows, the assumption of any other value of core temperature would only linearly shift the value of g, the heat generation per unit volume. Differences in g would be exacerbated if small animals maintained core temperatures in winter that were lower than those of larger animals. We assumed the environmental conditions are constant at 0°C for air and radiant temperatures and the wind is $0{\cdot}1$ m s^{-1}. These calculations allow us to compare heat loss from animals possessng the fur of a deer mouse or a red deer. At a weight of 10 g (the left-most data points for open and closed symbols in Fig. 20), it is clear that a mouse would have a greater benefit changing its fur for red deer fur than changing its body size from 10 to $21{\cdot}5$ g However, the long fur of red deer on a 10-g mammal would probably impede locomotion, since it is longer than the

length of the limbs of the animals. A 10-g animal might trip itself on such fur. Thus, a change in body size is virtually the only option left for animals whose body size is less than 40 g. As body size increases beyond 40 g, changes in fur properties make relatively little difference in weight-specific metabolic expenditures. Thus, a large animal like a red deer may have selective forces affecting both fur properties and body size. Red deer might benefit thermally from changes in both.

The 'usual' explanation for body-size changes with latitude in the literature has been couched in terms of reducing surface:volume ratios to reduce (relative) heat loss in a cool environment. However, as Equation 1 illustrates, it is the radial dimension squared that is the only non-linear variable affecting heat generation per unit volume, g.

Equation 1 is also useful to show that for a constant core–skin temperature gradient, as the radius increases, heat generation per unit volume, g, must decrease non-linearly. Thus, in steady state, a large animal *must* maintain a low metabolic rate, a small radius animal *must* have a high metabolic rate (or very long fur).

Mouse-to-elephant curve

One of the most intriguing aspects of animal metabolic rate is the 'mouse-to-elephant' curve. A great deal has been written about it, but there has been no first principles calculation of that curve. Calculations done with the endotherm model that estimate the mouse-to-elephant curve using the bounding allometries of a sphere and a cylinder approximation are illustrated in Fig. 21. To explore the possible impact of a small mammal *v.* a large mammal fur type, the fur of the red deer and deer mouse has been used in separate calculations for all body sizes. The calculations are for hypothetical animals of different body weights whose surface areas follow Meeh's equation. The cylinder calculations assumed body length twice that of the body diameter.

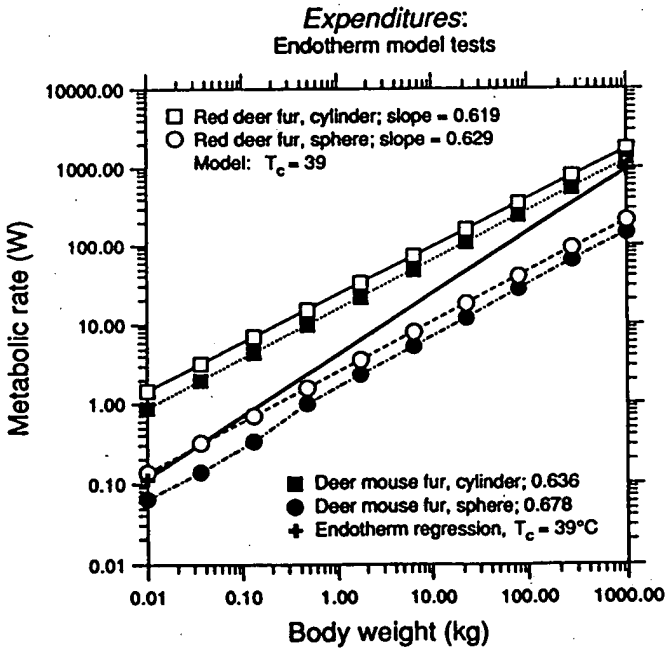

Fig. 21. Mouse-to-elephant metabolic rate calculations for cylindrical and spherical geometries and red deer fur *v.* deer mouse fur. The regression curve for the empirical data is the heavier centre line between the bounding calculations.

The empirical mouse-to-elephant curve is plotted as a heavy line between the two bounding calculations for curled-up and extended postures. Inspection of the results shown that body posture has much more impact than fur type, since sphere calculations using the fur of the deer mouse and the red deer both lie below the empirical data. Cylinder approximations with the two fur types both lie above the data. The r^2 coefficients for the regressed fit of the calculations against the individual points are greater than 0·999. It is not clear why the mouse-to-elephant curve, which has a slope of 0·75, lies close to the spherical posture for small animals and close to the extended posture for large animals. One possible explanation is that empirical measurements on small animals were done on animals that were more frequently curled up or lying down in metabolic chambers, whereas larger animals may have been standing wearing masks, instead. Another possibility is that the assumption in the calculations of a constant ratio of body length equal to twice body diameter may in fact change with body weight in animals. Nonetheless, it is reassuring that in this first crude approximation, it is possible to at least bound the empirical data.

Climate–disease–toxicant interactions affecting growth and reproduction potential

Interactions of multiple low-level stressors such as climate, disease, and toxicants can affect animal energetics in a number of ways. In two dimensions the typical curve for endotherms relating 'environmental temperature' to metabolic cost, whether that be in units of oxygen consumption per time or in terms of mass or energy needed per unit time to meet metabolic expenditure demands, is shown in Fig. 22. There is the usual U-shaped curve for

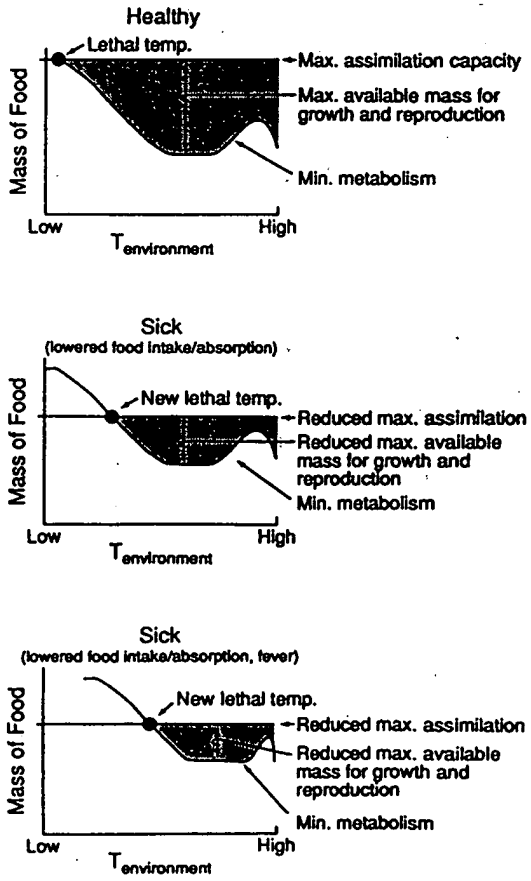

Fig. 22. Two-dimensional representation of 'environmental temperature', disease and toxicant effects on endotherm energetics. Food mass (energy) absorbed and food mass (energy) expended to meet metabolic needs specify the mass (energy) remaining for growth, reproduction or storage. A reduction in food absorbed as a result of reduced food availability, reduced appetite or disease not only reduces discretionary mass and energy, but puts the animal in a negative mass and energy balance for the coldest environmental conditions (those to the left of the intersection of the absorption and expenditure curves). Presence of a fever raises the expenditure curve and shifts it to the right. This further reduces discretionary mass and puts the animal in a negative mass and energy balance for more-moderate environments because the point of intersection of the two curves shifts to higher temperatures.

thermoregulatory metabolism. At low temperatures, metabolic rate must be high to maintain body temperature. At intermediate temperatures when animals are in the 'comfort' or 'thermoneutral' zone, metabolic rates might be at a minimum for a resting animal. At high temperatures, metabolic rate again climbs as heat stress induces higher metabolic expenditures associated in part with greater evaporation, circulation rates and the physical chemistry of biochemical reactions (the Q_{10} effect). Food absorption, theoretically a nearly horizontal line above the metabolism curve, although in practice somewhat environmentally temperature dependent, specifies energy available to the animals. The difference between the two lines represents the mass and energy available for growth and reproduction as originally proposed by Brody (1945).

These two lines change relative to each other when an animal is either sick or affected by toxicants (Fig. 22). Two changes occur when fever appears in an animal. First, the lower U-shaped metabolism curve rises vertically and shifts to the right because of a higher metabolic rate and regulation at higher body temperatures. The other change that typically occurs is that the ingestion/absorption of food declines (due to inability to find/capture food or appetite loss) and so the upper horizontal line drops toward the lower metabolism curve. This results in two changes in the overall energetics of the animal. First, the discretionary mass and energy available for growth and reproduction (Fig. 22) is more constrained. Second, the intersection of the mass (energy) absorbed and the mass (energy) expended curves shifts to a higher temperature such that at very low temperatures, the animal is in a negative mass (energy) balance. Thus, the allowable environments where the animal can remain in a positive mass balance decline as infections induce changes in mass (energy) intake and expenditures of animals.

The changes described for infections in many cases also apply to exposure to low-level pesticides and other environmental chemicals. A wide variety of chemicals are now implicated in changes in physiological and developmental parameters in animals (Colborn and Clement 1992). These changes include suppression of the immune parameters, alterations in nervous system functions, and changes in endocrine function (Amdur *et al.* 1991). Thus, elevation of thyroxine as a result of herbicide/insecticide exposure elevates metabolic rate (Porter *et al.* 1993) and changes immune parameters that may make an animal more vulnerable to infection or prolong an infection (Boyd *et al.* 1990), and will have effects similar to those of infections that arise as a result of exposure to pathogens without environmental chemicals being involved. Simultaneous effects on spatial discrimination and learning abilities (Boyd *et al.* 1990) could affect ability to find and obtain food, thereby also affecting energy and mass balances and possibly courtship and mating.

The energetics of a healthy animal (upper) with one that is stressed by disease or a toxicant (lower) in the context of measureable environmental variables, rather than 'environmental temperature', are compared in Fig. 23. The upper half of the Fig. for the healthy animal shows that increasing infrared and solar radiation (back to front) and increasing air temperature (left to right) affects metabolic rate and food needed to meet the metabolic demand (vertical axis) so as to form a surface with a trough running diagonally from the closest corner to the far corner. This trough represents the thermoneutral zone seen in the previous graph. A line on the surface from upper left to lower right traces the curve often seen in data from metabolic chambers where air and radiant temperatures are typically the same. All other possible combinations of air and radiant temperatures form the remainder of the surface. The angle of the trough relative to the horizontal coordinates depends upon wind speed and body size of the animal. At high wind speeds and/or smaller body sizes, the trough tends to be oriented perpendicular to the air temperature axis. In contrast, at very low wind speeds and/or very large body sizes, the surface rotates clockwise so that the trough tends to be oriented normal to the radiation axis instead (Porter 1989*a*). These rotations of the dish are due to changes in thickness of the boundary layer affecting convective heat transfer. The upper surface on the top of the graph that lays horizontally

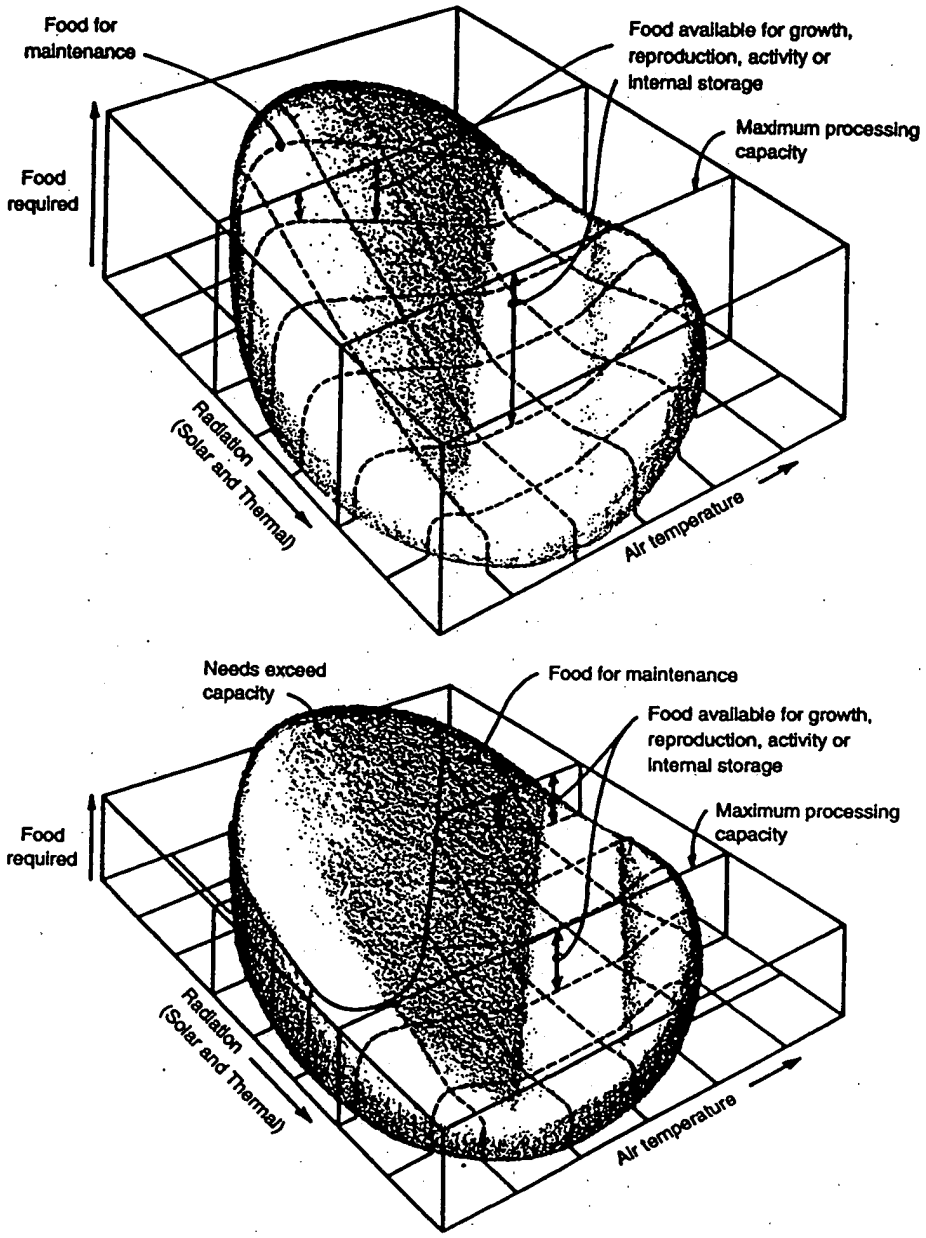

Fig. 23. Three-dimensional representation of climate, disease and toxicant effects on an endotherm's mass and energy balance. Increasing solar and infrared radiation from front to back *v.* increasing air temperature from left to right affect mass (energy) needed for metabolism (bottom to top). Mass (energy) absorbed is represented by the flat surface lying on top. The thermoneutral 'trough' angle relative to the two horizontal axes is determined by the boundary-layer thickness of the animal. Both wind speed and body size affect boundary-layer thickness. The top half of the Fig. represents a healthy animal. The bottom half of the Fig. represents conditions when an infection or toxicant raises metabolic rate and affects appetite and/or ability to find or capture food. Discretionary mass (energy) declines and colder environments now represent negative mass and energy balance conditions, where the lower surface pushes through the upper food absorption surface.

across the top, 'the lid', represents maximum food-processing capacity of the animal and the space between its surface and the lower 'floppy dish' represents mass available for growth, reproduction or fat storage.

The lower half of Fig. 23 illustrates what happens when fever is induced. The lower floppy dish rises and shifts to the right as seen by the position of the trough, which is shifted to the right relative to the trough in the top half of the figure. The other surface (the lid) has dropped due to a reduction in ability to either capture, digest or absorb food. Thus, part of the floppy dish protrudes through the lid representing a negative mass balance condition. The environmental conditions that allow the dish to lie below the lid are more restricted and the space between the dish and lid is compressed, representing a reduction in available mass and energy for growth, reproduction or fat storage. Thus, any toxicant or disease that alters metabolic rate or food-processing capacity or both could have its effect quantified for any environmental condition. Thus, it is possible to assess quantitatively the effects of simultaneous climate, disease and toxicant stresses on animal energetics and population dynamics.

Animal 'design'; genetic engineering

The endotherm model can explore effects of changes in fur properties on energetic requirements for different body sizes. Changes in pelt depth at different body sizes affect energetic requirements for different sizes of animals (Fig. 24). In general, as pelt depth increases, there is a reduction in metabolic cost at any given body size. At intermediate pelt depths there is a greater reduction in metabolic rate needed to maintain a core temperature over a relatively narrow range of change in pelt depth. This effect is greater the larger the animal.

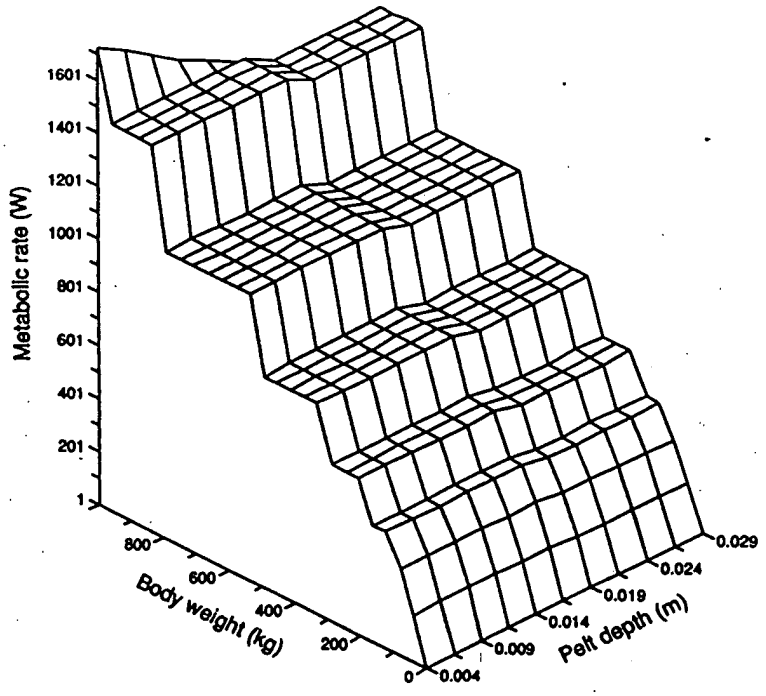

Fig. 24. Calculated effect of changing pelt depth and body size of red deer fur in summer on metabolic rate, using Meeh's equation for surface area as a function of body mass.

Changes in hair density at increasing body size can also affect metabolic expenditure (Fig. 25). Here, we have a figure somewhat reminiscent of a 'batmobile.' At the lowest hair densities, the fur no longer acts like a porous media, but rather like fur that does not exist. At the lowest densities, the skin is the primary focus of heat exchange. As hair density increases to very high densities, heat loss again increases substantially for all body sizes because the hair fibres, which are about eight times greater in thermal conductivity than the air between them, are so densely packed that they effectively become a solid insulation.

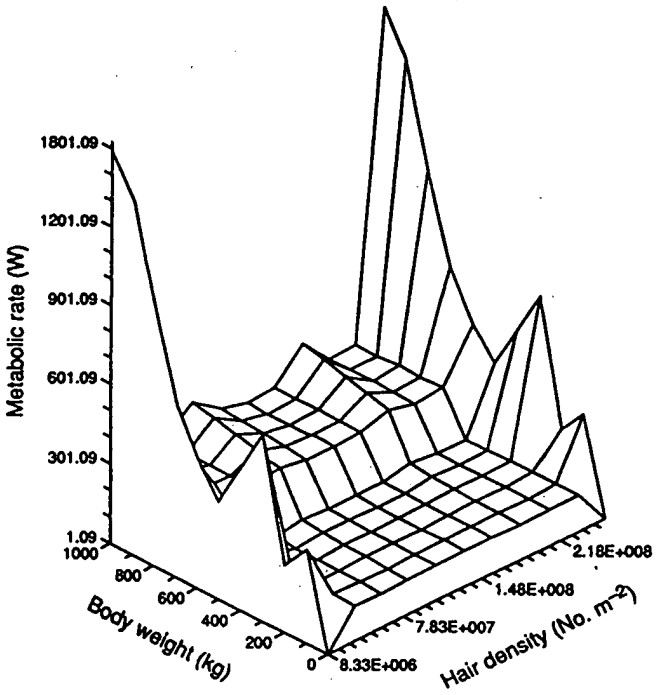

Fig. 25. Calculated effect of changing hair density and body size of red deer in summer on metabolic rate.

Thus, in designing animals by genetic-engineering techniques, certain combinations of hair density and depth might be avoided if minimisation of energetic cost is the goal.

Applications to community structure

We propose that these kinds of models might be used in combination with optimisation models, gut allometry and function models, and foraging energetics (locomotion costs) models to specify optimal body size for different environments varying in food distribution seasonally and from year-to-year. For a particular combination of these variables species B in Fig. 26 might be the optimal body size to minimise energetic costs and maximise growth and reproduction potential. This would result in a maximum or larger number of individuals of that particular species. However, since climates vary seasonally and from year to year and food distribution changes as it is harvested, other times of the year might present different optimal body size conditions. We propose that the patterns of change in a habitat as well as the habitat structure, which can influence microclimates available to animals, may dictate predictable assemblages of the numbers and sizes of species that ought to be present.

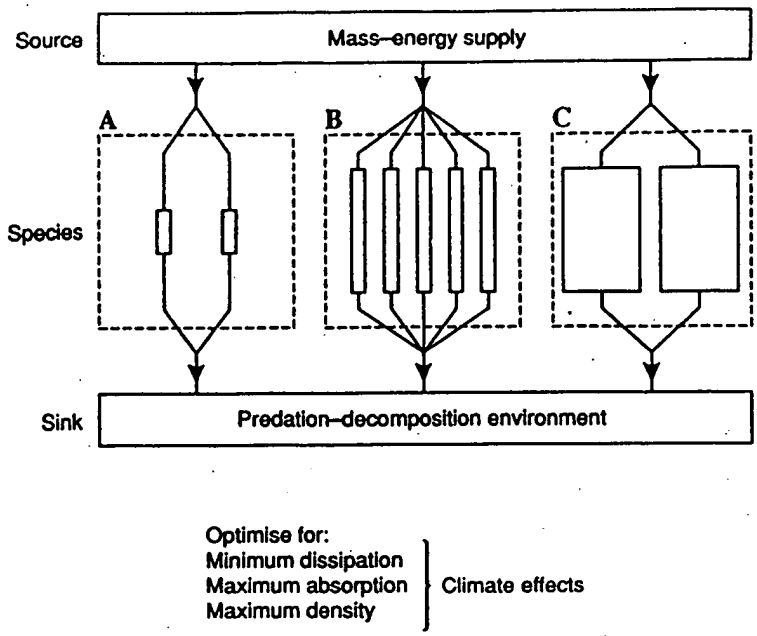

Fig. 26. Schematic of how energetic models coupled with body-size effects on gut function and locomotory costs may specify optimal body size that maximises reproduction. Seasonal and year-to-year variation in food distribution may specify a 'moving target' of optimal body size that maximises reproduction, thereby affecting community structure and dynamics through time.

Climate, vegetation, and food distribution characteristics are definable and energetic responses of animals are predictable. Life history parameters that are undoubtedly influenced by both genetic and environmental mechanisms can be integrated to build predictive models for population and community responses to environmental stresses of many different kinds.

Discussion

The results presented here indicate that, when used with appropriate geometric approximations, a porous-media fur model coupled with a model of internal heat generation throughout the body can give reasonable predictions of metabolic rates of endotherms.

The results also show the importance of behaviour and posture. Behaviour and posture affect surface area exposed to the environment, which affects heat loss and therefore affects 'conductance'. Various workers (McNab 1980) have relied heavily on conductance differences that could be due in part to postural differences during measurement to make inferences about various aspects of animal biology. Conductance calculations have been common in the physiological literature for mammals and birds. Unfortunately, observations of posture changes during metabolic measurements typically are not done. Thus, experimental data may include curled-up and extended postures in the same data set, which the endotherm models indicate can affect heat loss.

Because endotherms in the field can assume a range of postures and behaviours, the models can only be used to place bounds on the range of feasible metabolic expenditures, or on the food intake needed to meet those expenditures, if data are available on digestive physiology and types of food consumed.

Despite the inability to exactly calculate the metabolic rate at any instant, the ability to calculate the feasible range of variation is useful, especially if the calculations are to be used to estimate field energy expenditures and to try to extend those estimates to populations of endotherms.

These models can be applied to theoretical problems showing the basis for Bergmann's rule, predicting the mouse-to-elephant curve, and exploring optimality in the evolution of fur properties for different body sizes (McClure and Porter 1983; Gebremedhin *et al.* 1984; Webb *et al.* 1990). The models can be used to explore energetics in the context of climate change or pathogenic infections that induce body temperature changes. The models reduce the need for extensive physiological experimentation to determine temperature-dependent metabolic changes.

The models also have applications to conservation biology, by allowing one to obtain measured physical properties and behavioural characteristics of animals as input to biophysical–physiological–behavioural models to estimate energetics for new habitats or climate change scenarios. Several decades ago wildlife biologists made climate diagrams for species, hoping to predict the success of introductions. This current type of integrated approach using individual-based models to infer aspects of population dynamics is a logical refinement over old approaches and has been very fruitful in fisheries research (Kitchell *et al.* 1977) and in recent studies of lizard energetics and life histories (Grant and Porter 1992; Adolph and Porter 1993).

The models published here do not include calculations for solar radiation, although that problem has been solved (Kowalski 1978). It appears that at high solar intensities and with appropriate color patterns in fur, significant temperature gradients can be generated in fur that may promote convective heat transfer at low external wind velocities. Thus, a combined solar-convection model must be added to these models to simulate all possible weather conditions endotherms could encounter. A model of convective transport through fur has been developed (Stewart *et al.* 1993). This first principles convection model can be used to calculate heat and water transport through dry and wet fur.

Conclusions

The energetics of animals are driven by a limited, definable, measurable set of interconnected environmental variables and physical, physiological and behavioural properties of animals. These variables are interconnected in their effects on metabolic rate, water loss and potential for growth, reproduction and fat storage (Porter 1989*a*). This is particularly true for endotherms with porous insulation, where all the fur or feather heat-transfer process rates depend simultaneously on all others. This paper describes three different simultaneous measures of metabolic rate in the deer mouse in metabolic chambers and compares them with a model, EZFUR, that calculates metabolic rate on the basis of (1) core temperature measured by radio-telemetry, (2) the allometry of the animals, (3) their range of postural behaviours from spherical to cylindrical geometries, and (4) environmental conditions of air and radiant temperature, and wind speed. The model calculations bound the experimental data and suggest that curled-up postures predominate at low temperatures and extended postures predominate at higher air and radiant temperatures in metabolic chambers.

EZFUR predicts significant differences in slope of metabolic rate needed to maintain a constant core temperature over a range of air temperatures for curled-up *v.* extended postures. Thus, empirical estimates of heat transfer using calculated 'conductances' from oxygen consumption in metabolic chambers can be misleading because behaviour can change surface area exposed to the environment.

The endotherm models can be applied to a variety of theoretical and applied problems. They are generalisable and require minimal data obtainable at relatively modest cost.

We have illustrated here that one can quantitate the relative contributions of body size, fur properties, environmental conditions and regulated core temperature for their effects on animal energetics. Potential genetic engineering 'design' changes in body size, fur properties or fat content of animals and their effects on energetics can be evaluated. Effects on food consumption needed to maintain thermoregulation and potential for growth and reproduction can be evaluated. Finally, the models can be used to quantitatively evaluate energetics consequences of climate–disease–toxicant interactions, and to assess energetic constraints on community structure.

Acknowledgments

We gratefully acknowledge support through OHER in the Department of Energy DOE grant number DE-FG02-88ER60633 to W.P.P. We thank Katherine Nolan for technical help in the gas respirometry experiments, Robin McClellan and Bonita Lee for technical help in developing the gas respirometry, Steve Adolph, Raymond Huey and an anonymous reviewer for critically reviewing the manuscript. Raymond Huey provided the photo of Ray Cowles' fur-covered chuckwalla, and Bill Feeny did the illustrations. We thank Dr James Brown for ideas on application of the models to community structure.

References

Abramowitz, M., and Stegun, I. A. (1968). 'Handbook of Mathematical Functions.' (Dover Publications: New York.)

Adolph, S. C., and Porter, W. P. (1993). Temperature, activity and lizard life histories. *American Naturalist* **142**, 273–95.

Amdur, M. O., Doull, J., and Klassen, C. D. (1991). 'Toxicology: the Basic Science of Poisons.' (Pergamon Press: New York.)

Armitage, K. B., Melcher, J. C., and Ward, J. M. Jr (1990). Oxygen consumption and body temperature in yellow-bellied marmot populations from montane-mesic and lowland-xeric environments. *Journal of Comparative Physiology B* **160**, 491–502.

Bakko, E. B., Porter, W. P., and Wunder, B. A. (1988). Body temperature patterns in black-tailed prairie dogs in the field. *Canadian Journal Zoology* **66**, 1783–9.

Bird, R. B., Stewart, W. E., and Lightfoot, E. N. (1960). 'Transport Phenomena.' (Wiley & Sons: New York.)

Boyd, C. A., Weiler, M. H., and Porter, W. P. (1990). Behavioral and neurochemical changes associated with chronic exposure to low-level concentration of pesticide mixtures. *Journal of Toxicology and Environmental Health* **30**, 209–21.

Brody, S. (1945). 'Bioenergetics and Growth, with Special Reference to the Efficiency Complex in Domestic Animals.' (Reinhold Publications Corporation: New York.)

Budaraju, S., Stewart, W. E., and Porter, W. P. (1994). Prediction of forced ventilation in animal fur from a measured pressure distribution. *Proceedings of the Royal Society of London* (in press).

Calder, W. A. III. (1984). 'Size, Function and Life History.' (Harvard Uuniversity Press: Cambridge, MA.)

Cena, K., and Monteith, J. L. (1975*a*). Transfer processes in animal coats. I. Radiative transfer. *Proceedings of the Royal Society of London B* **188**, 377–93.

Cena, K., and Monteith, J. L. (1975*b*). Transfer processes in animal coats. II. Conduction and convection. *Proceedings of the Royal Society of London B* **188**, 395–411.

Cena, K., and Monteith, J. L. (1975*c*). Transfer processes in animal coats. III. Water vapour diffusion. *Proceedings of the Royal Society of London B* **188**, 413–23.

Cena, K., and Monteith, J. L. (1976). Heat transfer through animal coats. *Progress in Biometeorology* **1**, 343–51.

Colborn, T., and Clement, C. (1992). 'Chemically-induced Alterations in Sexual and Functional Development: the Wildlife/Human Connection.' (Princeton Scientific Publ. Co., Inc.: New Jersey.)

Conley, K. E., and Porter, W. P. (1986). Heat loss from deer mice (*Peromyscus*): evaluation of seasonal limits to thermoregulation. *Journal of Experimental Biology* **126**, 249–69.

Davis, L. B. Jr (1972). 'Energy Transfer in Fur.' p. 101. (College of Engineering, University of Kentucky, Lexington.)

Davis, L. B. Jr, and Birkebak, R. C. (1974). On the transfer of energy in layers of fur. *Biophysical Journal* 14, 249–68.

Degen, A. A., Kam, M., Hazan, A., and Nagy, K. A. (1986). Energy expenditure and water flux in three sympatric desert rodents. *Journal of Animal Ecology* 55, 421–9.

Gates, D. M. (1962). 'Energy Exchange in the Biosphere.' (Harper and Row Biological Monographs: New York.)

Gebremedhin, K., Cramer, C. O., and Porter, W. P. (1981). Predictions and measurements of heat production and food and water requirements of Holstein calves in different environments. *Transactions of the American Society of Agricultural Engineers* 24(3), 715–20.

Gebremedhin, K. G., Porter, W. P., and Warner, R. G. (1984). Heat flow through pelage of calves—a sensitivity analysis. *Transactions of the American Society of Agricultural Engineers* 27(4), 1140–9.

Grant, B. W., and Porter, W. P. (1992). Modeling global macroclimatic constraints on ectotherm energy budgets. *American Zoologist* 32, 154–78.

Kitchell, J. F., Stewart, D. J., and Weininger, D. (1977). Applications of a Bioenergetics Model to Yellow Perch (*Perca flavescens*) and Walleye (*Stizostedion vitreum vitreum*). *Journal of the Fisheries Board of Canada* 34(10), 1922–35.

Kleiber, M. (1975). 'The Fire of Life: an Introduction to Animal Energetics.' (Krieger Pub. Co.: Huntington, NY.)

Kovarik, M. (1964). Flow of heat in an irradiated protective cover. *Nature* 201, 1085–7.

Kowalski, G. J. (1978). An analytical and experimental investigation of the heat loss through animal fur. Ph.D. Thesis, Department of Mechanical Engineering, University of Wisconsin, Madison.

Kreith, F., and Black, W. Z. (1980). 'Basic Heat Transfer.' (Harper & Row.)

Lander, R. M. (1954). Gas is an important factor in the thermal conductivity of most insulating materials, Part II. Heating, piping and air conditioning. *Journal of the American Society of Heating and Ventilation Engineers*, 121–6.

Lapwood, E. R. (1948). Convection of a fluid in porous medium. *Proceedings of the Cambridge Philosophical Society* 44, 508–21.

McAdams, W. H. (1954). 'Heat Transmission.' 3rd Edn. (McGraw-Hill.)

McClure, P. A., and Porter, W. P. (1983). Development of insulation in neonatal cotton rats (*Sigmodon hispidus*). *Physiological Zoology* 56(1), 18–32.

McCullough, E. M., and Porter, W. P. (1971). Computing clear day solar spectra for the terrestrial ecological environment. *Ecology* 52, 1008–15.

McNab, B. (1980). Food habits, energetics, and the ppulation biology of mammals. *American Naturalist* 116, 106–24.

Mitchell, J. W. (1976). Heat transfer from spheres and other animal forms. *Biophysical Journal* 16, 561–9.

Mitchell, J. W., Beckman, W., Bailey, R., and Porter, W. (1975). Microclimatic modeling of the desert. In 'Heat and Mass Transfer in the Biosphere, Part I, Transfer Processes in the Plant Environment'. (Eds D. A. deVries and N. H. Afgan.) pp. 275–86. (Scripta Book Col: Washington, D.C.)

Moote, I. (1955). The thermal insulation of caribou pelts. *Textile Research Journal*, 25, 832–7.

Nagy, K. (1983). The doubly labeled water ($^3H_2^{18}O$) method: a guide to its use. Publication No. 12, p. 1417, University of California, Los Angeles.

Porter, W. P. (1969). Thermal radiation in metabolic chambers. *Science* 1661 (3901), 115–17.

Porter, W. P. (1989*a*). New animal models and experiments for calculating growth potential at different elevations. *Physiological Zoology* 62, 286–313.

Porter, W. P. (1989*b*). Program SOLRAD: software calculating clear sky diffuse and direct solar radiation for any location on earth. Distributed by WISCWARE. (U.W. Academic Computer Center, 1210 W. Dayton St., Madison, WI 53706.)

Porter, W. P., and Gates, D. M. (1969). Thermodynamic equilibria of animals with environment. *Ecological Monographs* 39, 245–70.

Porter, W. P., and McClure, P. A. (1984). Climate effects on growth and reproduction potential in *Sigmodon hispidus* and *Peromyscus maniculatus*. In 'Winter Ecology of Small Mammals'. (Ed. J. Merritt.) pp. 173–81. (Carnegie Museum of Natural History, Special Publication No. 10. Pittsburgh.)

Porter, W. P., Mitchell, J. W., Beckman, W. A., and DeWitt, C. B. (1973). Behavioral implications of mechanistic ecology: thermal and behavioral modeling of desert ectotherms and their microenvironment. *Oecologia* **13**, 1–54.

Porter, W. P., Parkhurst, D. F., and McClure, P. A. (1986). Critical radius in homeotherms. *American Journal of Physiology* **250** (*Regulatory Integrative Comparative Physiology* **19**), R699–R707.

Porter, W. P., Green, S. M., Debbink, N. L., and Carlson, I. (1993). Groundwater pesticides: interactive effects of low concentrations of carbamates aldicarb and methomyl and the triazine metribuzin on thyroxine and somatotropin levels in white rats. *Journal of Toxicology and Environmental Health* **40**, 15–34.

Press, W. H., Flannery, B. P., Teukolsky, S. A., and Vetterling, W. T. (1987). 'Numerical Recipes. The Art of Scientific Computing.' (Cambridge University Press: Cambridge.)

Rayleigh, Lord (1892). On the influence of obstacles arranged in rectangular order upon the properties of a medium. *Philosoptical Magazine* **34**, 481–502.

Robbins, C. T. (1983). 'Wildlife Feeding and Nutrition.' (Academic Press: New York, N.Y.)

Rowley, F. B., Jordan, R. C., Lund, C. E., and Lander, R. M. (1951). Gas is an important factor in the thermal conductivity of most insulating materials, Part I. Heating, piping and air conditioning. *ASHVE Journal*, 103–9.

Rubner, M. (1883). Uber den Einfluss der Korpergrosse auf Stoff- und Kraft-wechsel. *Zeitschrift für Biologie* **19**, 535–62.

Scheck, S. H. (1982). A comparison of thermoregulation and evaporative water loss in the hispid cotton rat, *Sigmodon hispidus texianus*, from northern Kansas and south-central Texas. *Ecology* **63**, 361–9.

Scholander, P. F., Hock, R., Walters, V., Johnson, F., and Irving, L. (1950). Heat regulation in some arctic and tropical mammals and birds. *Biological Bulletin* **99**, 237–58.

Siegel, R., and Howell, J. R. (1972). 'Thermal Radiation Heat Transfer.' (McGraw-Hill: New York.)

Skuldt, D. J., Beckman, W. A., Mitchell, J. W., and Porter, W. P. (1975). Conduction and radiation in artificial fur. In 'Perspectives in Biophysical Ecology'. pp. 549–58. (Springer Verlag: New York.)

Sokolov, V. E. (1982). 'Mammal Skin.' pp. 486–91. (University of California Press: Berkeley.)

Steudel, K. L., Porter, W. P., and Sher, D. (1994). The biophysics of Bergmann's rule: a comparison of the effects of pelage and body size variation on metabolic rate. *Canadian Journal of Zoology* (in press).

Stewart, W. E., Budaraju, S., Porter, W. P., and Jaeger, J. (1993). Prediction of forced ventilation in animal fur under ideal pressure distribution. *Functional Ecology* **7**, 487–92.

Tien, C. L., and Cunnington, G. R. (1973). Cryogenic insulation heat transfer. *Advances in Heat Transfer* **9**, 349.

Tracy, C. R., Welch, W. R., and Porter, W. P. (1980). 'Properties of Air. A Manual for Use in Biophysical Ecology.' 3rd Edn. p. 41. (Technical manual, U.W. Laboratory for Biophysical Ecology.)

Tregear, R. T. (1965). Hair density, wind speed, and heat loss in mammals. *Journal of Applied Physiology* **20**, 796–801.

Walsberg, G. E. (1988). Heat flow through avian plumages: the relative importance of conduction, convection and radiation. *Journal of Thermal Biology* **13**, 89–92.

Webb, D. R., Porter, W. P., and McClure, P. A. (1990). Development of insulation in juvenile rodents: functional compromise in insulation. *Functional Ecology* **4**, 251–6.

Wolf, S. (1966). A theory for the effects of convective air flow through fibrous insulations. (*Transactions of the American Society of Heating, Refrigeration and Air-conditioning Engineers* 2002: III.2.8.)

Wood, R. A., Nagy, K. A., MacDonald, N. S., Wakakuwa, S. T., Beckman, R. J., and Kaaz, H. (1975). Determination of oxygen-18 in water contained in biological samples by charged particle activation. *Analytical Chemistry* **47**, 646–50.

Appendix

Introduction

The goal of this appendix is to describe both a differential and integrated form of a porous-media heat-transfer model (hereafter call the 'fur model') for use in computing heat flux through fur and feathers. The original development by Kowalski (1978) was published as a Ph.D. thesis. Subsequent presentations of parts of the work in papers at national meetings (e.g. Kowalski and Mitchell 1979) were never published in the open literature. The fur model has undergone a number of changes and modifications, as well as extensive successful testing on species ranging in size from deer mice (Conley and Porter 1986) to Holstein calves (Gebremedhin and Porter 1981). The model has also been used successfully to estimate heat transfer through feathers in two species of birds (Shea and Porter, unpublished data), so it seemed particularly important to present the model structure in as clear a fashion as possible. The detailed derivation and added refinements described here have not been published elsewhere.

The differential form, LOFUR, has been implemented with a numerical integrator. Its advantage is that a variety of non-linear factors, such as variation of fur or feather density with depth, can be easily simulated. On the other hand, the integrated form, EZFUR, takes less computer time and provides an analytical solution that can be used to test the numerical model for simple situations.

The fur model involves equations from the skin out to the environment. Skin temperature is an important variable for the model that can be expressed in terms of core temperature and other variables in the equation for heat generation in a cylinder (Bird *et al.* 1960; Porter 1989*a*)

$$T_{core} - T_{skin} = \frac{gR^2}{4k} \tag{1}$$

a sphere (Bird *et al.* 1960)

$$T_{core} - T_{skin} = \frac{gR^2}{6k} \tag{2}$$

or an ellipsoid with semi-axex a, b and c (Porter, unpublished derivation)

$$T_{core} - T_{skin} = \frac{g}{2k}\left(\frac{a^2b^2c^2}{a^2b^2 + a^2c^2 + b^2c^2}\right). \tag{2}$$

Heat generation per unit volume, g, represents the metabolic rate needed to maintain a given core–skin temperature gradient for the radial dimension(s) of the flesh, R, and thermal conductivity, k. For simplicity of explanation, the derivation will focus on orthogonal coordinates for the fur, but the fur model developed in these coordinates is also satisfactory for cylindrical, spherical or ellipsoid coordinates. Application of the fur model to various body geometries will be apparent at the conclusion of the Appendix. For cylindrical and spherical geometries, the radius for computing convective heat transfer is R plus pelt depth. The implementation of the solution guesses for a value of g that balances the energy balance equation

$$Q_{gen} = Q_{fur}\,. \tag{4}$$

Total metabolical heat production, Q_{gen} (W), is the product of g from Equation 1 and the volume of the animal. Metabolic heat generated is lost primarily through the fur, if respiratory and ocular evaporative heat losses Q_{resp} and Q_{eyes} are negligible. If such terms are significant, Equation 4 becomes

$$Q_{gen} - Q_{resp} - Q_{eyes} = Q_{fur} \tag{5}$$

where

$$Q_{fur} = Q_c + Q_r\,. \tag{6}$$

The heat transfer by conduction through the fur, Q_c, is defined in Conley and Porter (1986) as

$$Q_c = \psi A_{skin} k_{eff}\left(C_1 \frac{T_{skin}}{z_L}\right) \tag{7}$$

where ψ is a dimensionless correction factor, k_{eff} is effective thermal conductivity, A_{skin} is the skin area, C_1 is an integration constant and z_L is the length of fur (m).

The heat transfer by direct and diffuse infrared radiation through the fur, Q_r, is (Conley and Porter 1986)

$$Q_r = \psi A_{skin} k_r \left(C_1 \frac{T_{skin}}{z_L} \right). \tag{8}$$

The task now is to specify the integration constant, C_1, defined below in terms of measurable variables. The other terms have been developed and defined in Kowalski (1978) and Conley and Porter (1986).

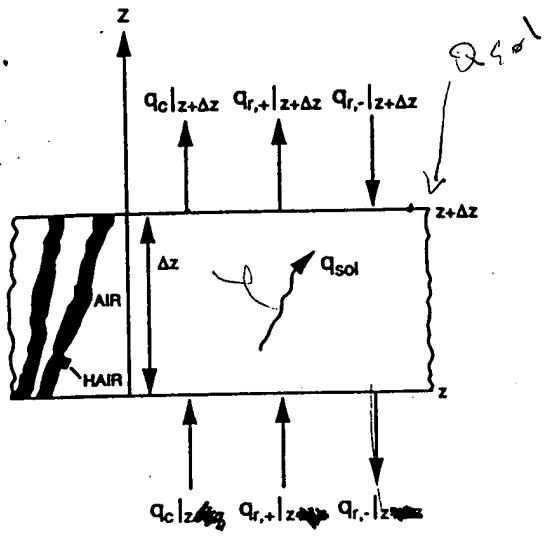

Fig. A1. System diagram of the fur.

Model Definition and Development of the Differential Form, LOFUR

The development of the fur model starts with a system diagram of the fur (Fig. A1). The figure establishes our frame of reference and specifies our assumptions. For any arbitrary volume element of thickness (Δz) in the fur we can write from the arrows in the diagram an energy balance for the heat flux per unit area

$$q_{in} = q_{out} \tag{9}$$

where

$$q_{in} = q_{c|z} + q_{r,+|z} + q_{r,-|z+\Delta z} + q_{sol} \tag{10}$$

and q_c is heat conducted per unit area, q_r is heat transfered by infrared radiation and q_{sol} is heat absorbed per unit area due to sunlight at any arbitrary depth.

The notation | means 'evaluated at' and the subscript $r,+$ and $r,-$ indicate radiation moving outward (away from the skin) and inwards (toward the skin) respectively.

Heat flux per unit area out of the element of thickness Δz is

$$q_{out} = q_{c|z+\Delta z} + q_{r,+|z+\Delta z} + q_{r,-|z}. \tag{11}$$

Substituting Equations 10 and 11 in Equation 9 and rearranging gives the following:

$$(q_{c|z+\Delta z} - q_{c|z}) + (q_{r,+|z+\Delta z} - q_{r,+|z}) - (q_{r,-|z+\Delta z} - q_{r,-|z}) - q_{sol}. \tag{12}$$

Dividing Equation 12 by Δz and taking the limit at $\Delta z \to 0$ results in

$$\lim \left[\frac{(q_{c|z+\Delta z} - q_{c|z})}{\Delta z} \right] + \lim \left[\frac{(q_{r,+|z+\Delta z} - q_{r,+|z})}{\Delta z} \right] - \lim \left[\frac{(q_{r,-|z+\Delta z} - q_{r,-|z})}{\Delta z} \right] = \frac{q_{sol}}{\Delta z} \tag{13}$$

which yields

$$\frac{dq_c}{dz}+\frac{dq_{r,+}}{dz}-\frac{dq_{r,-}}{dz}-q_{v,sol} \tag{14}$$

where $q_{v,sol}$ is the heat absorbed per unit volume (W m^{-3}) due to sunlight at any arbitrary depth.

The fur energy balance Equation 9 is now defined explicitly in terms of radiation and conduction heat fluxes, which are dominant heat-transfer mechanisms for most fur under common environmental conditions (Kowalski 1978). Note that the units of the equation are now heat flux per unit volume.

The form of the equation can be changed to use easily measured variables at known locations, i.e. at the skin and the outer boundary of the fur. The transformation of the equation starts with Fourier's Law

$$q_c=-k_{eff}\frac{dT}{dz} \tag{15}$$

where k_{eff} is the effective conductivity of the fur due to conduction processes as described in Conley and Porter (1986).

Taking the derivative of Equation 15 with respect to depth, z, yields

$$\frac{dq_c}{dz}=-k_{eff}\frac{d^2T}{dz^2}. \tag{16}$$

The radiant energy emitted upward from a surface through a participating medium (from the skin through the fur to any depth, z) is (Siegel and Howell 1972, p. 452)

$$q_{r,+}=2\sigma\{T_{skin}^4E_3[\beta_T z]+\int_0^z\beta_T T^4E_2[\beta_T(z-z^*)]dz^*\} \tag{17}$$

where σ is the Stefan Boltzmann constant (W m^{-2} K^{-4}), E_3 and E_2 are exponential integrals, β_T is an absorption, extinction coefficient (1/m) and z^* is a dummy integration variable.

The first term on the right in Equation 17 is the 'direct beam' infrared energy at any depth z that is travelling directly up through the fur and being attenuated by absorption described by the exponential integral, E_3. The second term on the right is the diffuse (scattered) radiation upward flux.

Taking the derivative of Equation 17 with respect to z to obtain a form consistent with the energy balance Equation 14 for the fur yields

$$\frac{dq_{r,+}}{dz}=2\sigma\{-\beta_T T_{skin}^4E_2[\beta_T z]+\beta_T T^4-\int_0^z\beta_T^2T^4E_1[\beta_T(z-z^*)]dz^*\} \tag{18}$$

where z^* is z_L-z and β_T is the absorption, emission coefficient in Bouger's (Beer's) Law

$$I=I_oe^{-rl}=I_oe^{-\beta_T z\cdot l}.$$

E is an exponential integral defined (Abramowitz and Stegun 1968) as

$$E_n(x)=\int_0^1\exp(-x/\mu)\mu^{n-2}d\mu$$

where μ is azimuth direction of hair fibres (radians), μ is cos Θ, s is $\frac{z}{\cos\theta}$ and A_p is A cos Θ.

The angle θ is measured as a zenith angle, that is, from a normal to the skin. Cos θ modifies the path length, s, for any θ greater than 0. The projected area of emission, A_p, from the horizontal plane for radiant energy travelling an equivalent vertical distance, z. These terms are used to evaluate β_T Kowalski (1978).

In similar fashion, infrared radiation in the downward direction directly from the sky plus the scattered downward flux in the fur is

$$\frac{dq_{r,-}}{dz}=2\sigma\{\beta_T T_{sky}^4E_2[\beta_T(z_L-z)]-\beta_T T^4+\int_z^{z_L}\beta_T^2T^4E_1[\beta_T(z^*-z)]dz^*\}. \tag{19}$$

Substituting Equations 16, 18 and 19 into Equation 14 gives the following:

$$k_{eff}\frac{d^2T}{dz^2} - 2\sigma\beta_T T_{skin}^4 E_2[\beta_T z] + 2\sigma\beta_T T^4 - 2\sigma\int_0^z \beta_T^2 T^4 E_1[\beta_T(z-z^*)]dz^* - 2\sigma\beta_T T_{sky}^4 E_2[\beta_T(z_L-z)] + 2\sigma\beta_T T^4 - 2\sigma\int_z^{z_L}\beta_T^2 T^4 E_1[\beta_T(z^*-z)]dz^* = q_{v,sol}\,. \quad (20)$$

By reformulating the heat flux Equation, 14, as an equation in terms of temperature, Equation 20, we get a form that will have easily measured variables when the equation is integrated. To get there we first solve for T as a function of z. This can be done numerically using a numerical integrator such as an Adams Predictor-Corrector or, if less accuracy is needed, a Runge-Kutta integrator. Boundary conditions must be specified. We can use physical conditions and assumptions about heat-transfer mechanisms to choose boundary conditions. For example, at $z=z_L$, the fur–air interface, the first boundary condition could be that heat conducted by the fur fibres and by the air between the fibres equals the heat exchange by convection,

$$q_{cond} = q_{conv}\,. \quad (21)$$

Substituting the mechanism equations for these two terms yields

$$-k_{eff}\frac{dT}{dz} = h_c(T_{z_L} - T_{air}) \quad (22)$$

where h_c is a convection heat transfer coefficient (W m^{-2} C^{-1}).

The second boundary condition (needed because of the second order derivative in Equation 20) could be at the other edge of the fur boundary, the skin, where $z=0$. Here

$$T_{z_o} = T_{skin}\,. \quad (23)$$

At this point we have concluded the formulation of the derivative version of the radiation–conduction model. Definitions of k_{eff} and other terms may be found in Kowalski (1978), McClure and Porter (1983) and Conley and Porter (1986). Equation 20 is implemented using an Adams Predictor-Corrector integrator for numerical solutions that accommodate a variety of linear or non-linear fur properties (density, diameter) as a function of depth (computer model LOFUR). A sensitivity analysis showed that those properties do not affect conduction–radiation heat transfer nearly as much as skin (core) temperature, air and radiant temperature (McClure and Porter 1983). A simpler linear model, EZFUR, has also been developed. Both are available for IBM compatible computers with math coprocessors from W.P.P. An analytical solution for Equation 20 is the basis for EZFUR described below.

Analytical Solution to the Radiation–Conduction Fur Model, EZFUR

The simplified version of the fur model assumes a linear temperature profile through the fur based on the Rossland diffusion approximation (Siegel and Howell 1972, p. 473).

$$T = C_1 z + C_0 \quad (24)$$

where T is the temperature at any depth, z, in the medium and C_1 and C_0 are constants to be evaluated. This equation is the general form, which will now need to be defined explicitly in terms of measurable variables.

To get an 'effective' or average fur temperature, $\bar{T}$ (°K), we need to integrate over the fur depth.

$$\bar{T} = \frac{\int_0^{z_L}(C_1 z + C_0)dz}{\int_0^{z_L} dz} = \frac{[C_1\frac{z^2}{2} + C_0 z]_0^{z_L}}{z|_0^{z_L}} \quad (25)$$

which yields

$$\bar{T} = \frac{C_1 z_L}{2} + C_0\,. \quad (26)$$

To evaluate C_0, we can use the boundary condition that at $z=0$, $T=T_{skin}$. Substituting this boundary condition into Equation 26, we get

$$T_{skin}=C_0 . \tag{27}$$

Substituting Equation 27 into Equation 26, we get

$$\bar{T}=\frac{C_1 z_L}{2}+T_{skin} . \tag{28}$$

We still must evaluate the integration constant, C_1. We can do that using the definition of heat loss from the fur at the fur–air interface as

$$q_{cond}+q_{r,-}=q_{conv}+q_{r,+} . \tag{29}$$

Substituting the definitions of each of the terms in Equation 29 we obtain

$$-(k_{eff}+k_r)\frac{dT}{dz}+\sigma T_{sky}^4=h_c(T-T_{air})+2\int_0^{z_L}\beta_T\sigma T^4 E_2[\beta_T z^*]dz^* . \tag{30}$$

We want to substitute measurable values for T in Equation 30. To compute heat transfer by convection, the temperature at the fur–air interface where $z=z_L$ is

$$T|_{z_L}=\frac{C_1 z_L}{2}+T_{skin} . \tag{31}$$

For radiation out, the diffuse flux and associated temperatures are

$$2\int_0^{z_L}\beta_T\sigma T^4 E[\beta_T z^*]dz^* . \tag{32}$$

Invoking the definition of the average fur temperature and moving all the constants outside the integral in Equation 32 results in

$$2\beta_T\sigma\bar{T}^4\int_0^{z_L}E_2[\beta_T z^*]dz^* . \tag{33}$$

Initially, we will define all the constants in front of the integral as the constant A for algebraic simplicity. We must also evaluate the exponential integral and put it in algebraic terms. To do this we use the definition of an exponential integral (Abramowitz and Stegun 1968).

$$\int E_n(x)=-E_{n+1}(x) . \tag{34}$$

Substituting Equation 34 into Equation 33, using A as the definition of the collection of constants, and remembering that $\int e^{ax}=\frac{1}{a}e^{ax}$,

$$A\int_0^{z_L}E_2[\beta_T z^*]dz^*=A\left[-E_3[\beta_T z^*]\cdot\frac{1}{\beta_T}\right]\Big|_0^{z_L} \tag{35}$$

$$=A\left[-\frac{1}{\beta_T}[E_3(\beta_T z_L)-E_3(0)]\right] . \tag{36}$$

The exponential integral for $x=0$ can be evaluated directly, since

$$E_n(0)=\frac{1}{n-1}\ \text{ for } n\geq 2;\ \text{thus } E_3(0)=\frac{1}{2} . \tag{37}$$

Thus, Equation 33 becomes

$$2\beta_T\sigma\bar{T}^4\left[\frac{1}{2\beta_T}-\frac{1}{\beta_T}E_3[\beta_T z_L]\right] \tag{38}$$

clearing fractions

$$\sigma\bar{T}^4(1-2E_3(\beta_T z_L)) . \tag{39}$$

We are almost ready to insert definitions into the fur–air heat balance equation. Noting from Equations 21 and 24 that

$$\frac{dT}{dz}=\frac{d(C_1z+C_0)}{dz}=C_1 \tag{40}$$

and substituting Equations 24, 27, 39 and 40 into Equation 30 we obtain

$$-(k_{eff}+k_r)C_1+\sigma T_{sky}^4=h_c(C_1z_L+T_{skin}-T_{air})+\sigma\bar{T}^4(1-2E_3(\beta_T z_L))\,. \tag{41}$$

The term $\bar{T}^4$ needs to be reduced to a first-order term to get the final equation in terms of measurable boundary conditions, as will be seen below. To achieve, this, we first subtract

$$\sigma(1-2E_3(\beta_T z_L))T_{sky}^4$$

from both sides of the equation, yielding

$$-(k_{eff}+k_r)C_1+\sigma T_{sky}^4-\sigma(1-2E_3(\beta_T z_L))T_{sky}^4=$$
$$h_c(C_1z_L+T_{skin}-T_{air})+\sigma(1-2E_3(\beta_T z_L))(\bar{T}^4-T_{sky}^4)\,. \tag{42}$$

Now we will linearise $\bar{T}^4$ and T_{sky}^4 about T_{ave}:

$$T_{ave}=\frac{T_{skin}+T_{sky}}{2} \tag{43}$$

using Taylor's series, $f(x)=f(a)+f'(a)(x-a)+f''(a)\frac{(x-a)^2}{2!}+\ldots$

$$\bar{T}^4=T_{ave}^4+4T_{ave}^3(\bar{T}-T_{ave})+\ldots. \tag{44}$$

$$T_{sky}^4=T_{ave}^4+4T_{ave}^3(T_{sky}-T_{ave})+\ldots \tag{45}$$

Subtracting Equation 45 from Equation 44 results in

$$\bar{T}^4-T_{sky}^4=4T_{ave}^3(\bar{T}-T_{sky})\,. \tag{46}$$

Substituting Equation 46 into Equation 42 results in

$$-(k_{eff}+k_r)C_1+\sigma T_{sky}^4-\sigma(1-2E_3(\beta_T z_L))T_{sky}^4=$$
$$h_c(C_1z_L+T_{skin}-T_{air})+\sigma[(1-2E_3(\beta_T z_L))4T_{ave}^3(\bar{T}-T_{sky})]\,. \tag{47}$$

We can substitute Equation 28, a definition of $\bar{T}$ into Equation 47 and prepare to solve for C_1 by first expanding the last term in Equation 47:

$$-(k_{eff}+k_{rad})C_1=\sigma(1-2E_3(\beta_T z_L))T_{sky}^4-\sigma T_{sky}^4+h_cC_1z_L+h_cT_{skin}-h_cT_{air}+$$
$$\sigma\left[(1-2E_3(\beta_T z_L))4T_{ave}^3\frac{C_1z_L}{2}+4T_{ave}^3T_{skin}-4T_{ave}^3T_{sky})\right]\,. \tag{48}$$

Factoring out C_1 and expanding the first term on the right in Equation 48 results in

$$C_1[-(k_{eff}+k_r)-h_cz_L-\sigma[(1-2E_3(\beta_T z_L))2T_{ave}^3z_L]=$$
$$\sigma T_{sky}^4-2E_3(\beta_T z_L)\sigma T_{sky}^4-\sigma T_{sky}^4+h_c(T_{skin}-T_{air})+4\sigma T_{ave}^3(1-2E_3(\beta_T z_L))(T_{skin}-T_{sky})\,. \tag{49}$$

Dividing both sides by the coefficient of C_1 and rearranging results in

$$C_1=-[4\sigma T_{ave}^3(T_{skin}-T_{sky})(1-2E_3(\beta_T z_L))+h_c(T_{skin}-T_{air})-2\sigma T_{sky}^4E_3(\beta_T z_L)]/$$
$$[(k_{eff}+k_r)+(h_c+2\sigma T_{ave}^3(1-2E_3(\beta_T z_L)))z_L]\,. \tag{50}$$

Notice that in the original differential Equation 30 the direct beam long wavelength radiation from the skin that reaches the fur-air interface is missing. This may be an important term, especially for animals with short or sparse fur. From the definition of $q_{r,+}$, Equation 17, that term is

$$2\sigma T_{skin}^4E_3(\beta_T z_L)\,. \tag{51}$$

Adding Equation 51, inserting the definition of T_{ave} and rederiving Equation 50 yields

$$C_1 = -[4\sigma\left(\frac{T_{skin}+T_{sky}}{2}\right)^3(T_{skin}-T_{sky})(1-2E_3(\beta_T z_L))+h_c(T_{skin}-T_{air})+2\sigma(T_{skin}^4-T_{sky}^4)E_3(\beta_T z_L)]/$$
$$[(k_{eff}+k_r)+(h_c+2\sigma\left(\frac{(T_{skin}+T_{sky})}{2}\right)^3(1-2E_3(\beta_T z_L)))z_L]\,. \quad (52)$$

Now that C_1 is defined in terms of measurable quantities, we can insert Equation 52 into Equation 31, solve Equation 31 for T_{skin}, and insert it into Equation 1. Solving for the heat generation per unit volume, we get

$$g=\frac{4k}{R^2}(T_c-T_{skin})=\frac{4k}{R^2}(T_c-(T|_{z_L}-C_1 z_L))\,. \quad (53)$$

The temperature evaluated at z_L in Equation 53 can be a simple assumption that the temperature at the fur–air interface equals air temperature. Alternatively, a more-sophisticated boundary-layer formulation can be inserted, which would vary as a function of body size and wind speed.

Implications for variables that affect metabolic rate in endotherms

Equations 52 and 53 illustrate how, in the absence of sunlight, metabolic rate depends on body diameter, pelt thickness, thermal conductivity, maintained core temperature, air temperature, and sky radiant temperature, all of which are embedded in C_1. Fur density, hair diameter and hair length affect β_T in C_1. Wind speed and body size effects also affect the temperature at the fur–air interface, $T|_{z_L}$, where an increase in wind speed can bring the temperature there closer to the free-stream air temperature outside the boundary layer. Pelt depth also affects body dimension, affecting boundary-layer thickness and convective heat transport, so a change in a single variable, like pelt depth, affects heat generation requirements in more than one term. Finally, surface area (affected by posture) is also important (note that C_1 is part of Equations 7 and 8, which include area exposed to the environment). Observations of posture are typically not made during measurements of metabolic rate.

Finally, it should be noted that Equation 52 considers only one radiant temperature. It is called 'sky', but could equally well be called 'wall' for metabolic-chamber measurements, where the walls are composed of some insulating material, such as glass, which does not reflect infrared radiation, or are painted with a non-conductive paint (Porter 1969). For animals outdoors, two radiant temperatures are typically involved, the sky and ground radiant temperatures. Thus, ground temperature, T_{grd}, could be substituted in Equation 52 for T_{sky} for calculations for the lower half of an animal.

This completes the solution of EZFUR, the linear model of radiation and conduction heat transfer in fur. Further modifications using a correction factor, ψ (Siegel and Howell 1972), were implemented by Kowalski and Mitchell (1979), in Conley and Porter (1986). The use of ψ allows for non-linear effects and results in excellent agreement with the numerical integration version of the model, LOFUR.

Manuscript received 27 September 1993; accepted 15 February 1994